Life Sciences 321 (2023) 121598

Contents lists available at ScienceDirect

Life Sciences

journal homepage: www.elsevier.com/locate/lifescie

Collagen matricryptin promotes cardiac function by mediating scar formation

Gabriel A. Grilo [a], Sirin N. Cakir [a], Patti R. Shaver [a], Rugmani P. Iyer [a], Kaitlin Whitehead [a], Joseph M. McClung [a,b,c], Ali Vahdati [d], Lisandra E. de Castro Brás [a,b,*]

[a] Department of Physiology, The Brody School of Medicine, East Carolina University, Greenville, NC 27834, United States of America
[b] Department of Cardiovascular Sciences, The Brody School of Medicine, East Carolina University, Greenville, NC 27834, United States of America
[c] East Carolina Diabetes and Obesity Institute, The Brody School of Medicine, East Carolina University, Greenville, NC 27834, United States of America
[d] Department of Engineering, East Carolina University, Greenville, NC 27858, United States of America

ARTICLE INFO

Keywords:
Myocardial scar
Matricryptin
Cardiac remodeling
Myocardial infarction

ABSTRACT

Aims: A peptide mimetic of a collagen-derived matricryptin (p1159) was shown to reduce left ventricular (LV) dilation and fibrosis after 7 days delivery in a mouse model of myocardial infarction (MI). This suggested p1159 long-term treatment post-MI could have beneficial effects and reduce/prevent adverse LV remodeling. This study aimed to test the potential of p1159 to reduce adverse cardiac remodeling in a chronic MI model and to elucidate p1159 mode-of-action.

Materials and methods: Using a permanent occlusion MI rodent model, animals received p1159 or vehicle solution up to 28 days. We assessed peptide treatment effects on scar composition and structure and on systolic function. To assess peptide effects on scar vascularization, a cohort of mice were injected with *Griffonia simplicifolia* isolectin-B4. To investigate p1159 mode-of-action, LV fibroblasts from naïve animals were treated with increasing doses of p1159.

Key findings: Matricryptin p1159 significantly improved systolic function post-MI (2-fold greater EF compared to controls) by reducing left ventricular dilation and inducing the formation of a compliant and organized infarct scar, which promoted LV contractility and preserved the structural integrity of the heart. Specifically, infarcted scars from p1159-treated animals displayed collagen fibers aligned parallel to the epicardium, to resist circumferential stretching, with reduced levels of cross-linking, and improved tissue perfusion. In addition, we found that p1159 increases cardiac fibroblast migration by activating RhoA pathways via the membrane receptor integrin α4.

Significance: Our data indicate p1159 treatment reduced adverse LV remodeling post-MI by modulating the deposition, arrangement, and perfusion of the fibrotic scar.

Abbreviations: Ab, Antibody; BW, Body Weight; CD31, Platelet Endothelial Cell Adhesion Molecule 1; cDNA, Complementary DNA; CO, Cardiac Output; Ct, Threshold Cycle; D0, Day 0; D7, Day 7; D14, Day 14; D21, Day 21; D28, Day 28; ECM, Extracellular Matrix; EDV, End-Diastolic Volume; EF, Ejection Fraction; ESV, End-Systolic Volume; FBS, Fetal Bovine Serum; FS, Fractional Shortening; GS-IB4, Griffonia simplicifolia isolectin-B4; GTP, Guanosine Triphosphate; HF, Heart Failure; HFpEF, Heart Failure with Preserved Ejection Fraction; HFrEF, Heart Failure with Reduced Ejection Fraction; HR, Heart Rate; Itg, Integrin; Itga3, Integrin alpha 3; Itgα4, Integrin alpha 4; Itgam, Integrin Subunit Alpha M; Itgb1, Integrin Beta 1; Itgb2, Integrin Beta 2; Itgb3, Integrin Beta 3; LAD, Left Anterior Descending Coronary Artery; LOX2, Lysyl Oxidase; LV, Left Ventricle; LVAWd, Left Ventricle Anterior Wall End Diastole; LVAWs, Left Ventricle Anterior Wall End Sistole; LVIDd, Left Ventricle Internal Diameter End Distole; LVIDs, Left Ventricle Internal Diameter End Sistole; LVPWd, Left Ventricle Posterior Wall End Diastole; LVPWs, Left Ventricle Posterior Wall End Sistole; m.o., Month old; MI, Myocardial infarction; MMP, Matrix metalloproteinase; OCT, Optimal cutting temperature; OPN, Osteopontin; P2, Passage 2; PBS, Phosphate Buffered Saline; PSR, Picro-Sirius Red; PVDF, Polyvinylidene Difluoride; qPCR, Quantitative Polymerase Chain Reaction; RhoA, Ras Homolog Family Member A; RhoGDIα, Rho GDP-Dissociation Inhibitor 1 Alpha; RNA, Ribonucleic Acid; RV, Right Ventricle; s.c., subcutaneous; SFM, Serum Free Media; SV, Stroke Volume; TGF-β, Transforming Growth Factor-Beta 1; W/D, Wet to Dry.

* Corresponding author at: The Brody School of Medicine, East Carolina University, 600 Moye Blvd., Mail stop 634, Greenville, NC 27834, United States of America.

E-mail address: decastrobrasl14@ecu.edu (L.E. de Castro Brás).

https://doi.org/10.1016/j.lfs.2023.121598
Received 3 January 2023; Received in revised form 7 March 2023; Accepted 15 March 2023
Available online 22 March 2023

1. Introduction

The lifetime risk of heart failure (HF) remains high; after 45 years of age, HF rate varies across racial and ethnic groups from 20 % to 45 % [1]. Moreover, the 5-year mortality for those with HF remains high (39.4 % overall; 24.4 % for those 60 years of age and 54.4 % for those 80 years of age) [1,2]. Each year 1.2 million Americans have a myocardial infarction (MI) and the risk for recurrent MIs is above 25 % [3]. Negative prognosis after MI is mostly due to left ventricular adverse remodeling and, despite significant advances in its treatment, MI remains the most important cause of HF [4]. The annual economic impact of $150 billion associated with this disease makes it a research priority [5,6]. After an MI, the infarcted area is replaced by an exaggerated fibrotic scar, which decreases the heart's contractility [7]. Fibrosis in the left ventricle (LV) post-MI reduces hemodynamic capacity, resulting in compensatory hypertrophy of the survivor cardiomyocytes in an effort to restore and maintain LV performance [8]. The extent of myocardial remodeling post-MI associates with the patient's final prognosis and the evolution of the resulting scar depends on the interaction between cardiac cells and the extracellular matrix (ECM). Understanding the mechanisms involved in adverse LV remodeling post-MI is highly desirable for the development of new therapeutic approaches.

Matricryptins are bioactive fragments proteolytically released from ECM proteins [9]. Several matricryptins have been shown to regulate physiopathological processes, including angiogenesis, tumor growth, and cell migration [10,11]. Natural matricryptins and mimetic synthetic peptides currently are being investigated both in vitro and in animal models as promising anti-cancer drugs. For instance, administration of metastatin in vivo was inhibitory to tumor growth and local angiogenesis [12]; in a mouse model of bleomycin-induced lung fibrosis, genetic depletion of FBLN1C1 (a fibulin 1 matricryptin) protected animals from developing airway and lung remodeling and fibrosis by attenuation of the TGFβ signaling pathway and myofibroblast differentiation [13]. Since ECM degradation is a hallmark of tissue healing and remodeling, the generation of myocardial matricryptins and their roles post-MI are of high interest for the cardiac regenerative field.

Our laboratory identified a collagen-derived matricryptin (C-1158/59) that gradually forms post-MI both in humans and mice [14]. Importantly, increasing levels of C-1158/59 associated with lower left ventricular (LV) filling pressure in post-MI patients, suggesting a beneficial role for C-1158/59. Indeed, our lab found that post-MI mice treated for 7 days with p1159, a peptide mimetic of C-1158/59 cryptic site, displayed less collagen deposition and an increase in local blood vessel network, which resulted in reduced LV dilation [14]. These data suggest that p1159 therapy post-MI may modulate the fibrotic scar formation. However, its mechanisms of action are still unknown. The goals of this study were two-fold: 1) To identify the receptor and signaling pathway(s) activated by p1159 and 2) Test the hypothesis that p1159 long-term therapy leads to attenuated adverse LV remodeling post-MI.

2. Methods

2.1. Inclusion and exclusion criteria

For the MI experiments, inclusion criteria included: confirmation of MI by both blanching and lack of movement of the LV downstream of ligation, infarct size >40 % and ejection fraction (EF) below 40 % at day 7 post-MI. Animals were excluded when MI was not confirmed either during surgery (visual observation and lack of ST elevation on ECG) or 3 h after ligation (by echocardiography), when infarct size was lower than 40 % (quantified by strain analysis), and when EF was above 40 % at 7 days post-MI. We also excluded animals that died within 24 h of surgery. Perioperative death within 24 h of MI in nonreperfused mice is usually due to surgical errors (e.g., excessive bleeding or lung injury) or very large infarct sizes and lethal arrhythmias [15].

2.2. Animals

All experiments using vertebrate animal were conducted according to the "Guide for the Care and Use of Laboratory Animals" [16] and were approved by the Institutional Animal Care and Use Committee at the East Carolina University in our fully accredited animal facility. Both male and female C57BL/6 mice (Charles River stock #027), 4 to 6 m.o., were used in this study (n = 5–6/sex SHAM; n = 10–14/sex/treatment).

2.3. Permanent occlusion of coronary artery

Approximately 20 % of patients are hospitalized too late to receive reperfusion therapy or due to other diseases are not eligible for reperfusion [3]. These patients will have an occluded artery that blocks the blood flow to part of the LV and this can result in infarct sizes up to 45 % of the LV [17,18]. Accordingly, to mimic these human clinical settings, an infarct size of 40–50 % was induced by permanent occlusion of the left anterior descending coronary artery (LAD). Animals received treatment 3 h after infarction via an osmotic pump, implanted subcutaneously on the animals' back containing either p1159 (14 μg/day/kg body weight) or saline solution (vehicle). Coronary ligation of the LAD was performed as previously described [14]. Animals that were used as SHAM controls went through the same surgical procedures but without suturing the LAD.

2.4. Functional measurements and tissue collection

Echocardiograms were acquired 3–4 times for each animal, at baseline (D0) and every 7 days post-MI until sacrifice at either day 14 (D14) or day 28 (D28). MI was validated at D7 and animals with an EF < 40 % were included in the study. After echocardiography, the infarcted heart was harvested in full diastole and the LV and the right ventricle (RV) were separated. The LV was sectioned in three parts: base (remote zone), middle (border zone), and apex (infarcted zone). The infarcted apex and the remote, non-infarcted, tissue were snap frozen in liquid nitrogen and stored at −80 °C for RNA extraction. The border zone was fixed in 10 % formalin and processed for histological analysis.

2.5. LV histological collagen quantification

LV sections were stained with Picrosirius Red (PSR) for collagen quantification as previously described [14]. Total collagen (bright pink/red stain) was quantified by a blinded individual using Image-Pro Premier Offline 9.1 Software (Media Cybernetics, Maryland). The total collagen was quantified in each image individually in the infarcted and border zones, averaged, and presented as percentage of area stained.

2.6. Collagen fiber orientation

To determine how collagen fibers remodel after MI with time and whether p1159 treatment affects fiber alignment, we determined fiber orientation during early remodeling (D7), mid-remodeling (D14), and late remodeling (D28). PSR-stained slides were used and images were acquired using a birefringence filter. All images were rotated until the epicardial margin reached an angle of 0° for circumferential angle normalization. The collagen fibers orientation (vector angles) were determined using previously published image-processing code MatFiber for automated fiber orientation analysis based on maximum intensity gradients [19] and implemented in MATLAB (version R2019B, MathWorks, Natick, MA) [20]. Average alignment of fibers was determined by measuring the angles between −90 and +90° (in 10° orientation bins) in subregions of the image and reporting the angular histograms of average alignment. Fractions were plotted either by individual area - infarcted zone and border zone - or combined area.

2.7. Protein analysis

We performed immunoblots against collagen 1, collagen 3, decorin, lysyl oxidase, periostin, osteopontin, and integrin alpha 4. Total protein staining was used for normalization, once protein levels change after MI impeding the use of a control protein.

2.8. Vessel quantification

A cohort of animals was treated ± p1159 for 14 days post-MI and vessels labeled with lectin for visualization of the vasculature in the infarcted zone. Two hours prior to sacrifice, 50 μL of 1 mg/mL of *Griffonia simplicifolia* isolectin-B4 Dylight594 conjugate (#DL-1207, Vector) was injected into the retro-orbital sinus using a 31-gauge needle. The middle LV section was frozen in liquid nitrogen and embedded later in OCT medium for cryosectioning. Ten micrometer thickness sections were obtained, fixed in 1:1 methanol/acetone solution for 10 min at −20 °C, rehydrated in 1xPBS, and blocked with 5 % bovine serum albumin in 1xPBS for 1 h at room temperature. Tissues were incubated with CD31 antibody 1:100 dilution (#MCA2388GA, Bio-Rad) overnight at 4 °C; the next morning slides were incubated with Alexa-Fluor secondary antibody 1:250 dilution (Invitrogen) for 1 h to counterstain the total vessels. Sections were mounted with Vectashield DAPI (Vector) medium and 3 random images of the ventricular wall from each sample were captured using an Olympus IMT-2 fluorescent microscope. CD31 was detected in green color using FITC filter (470 nm excitation) and Dylight594 was visualized in red color using a TxRed filter (585 nm excitation). Percentage of stained areas were quantified using ImageJ with standard threshold limits for each filter.

2.9. LV fibroblast isolation and culture

Naïve mice were euthanized with an overdose of inhalational isoflurane and the heart removed. The LV was isolated, rinsed in sterile saline solution, and weighted. Minced LVs were dissociated into single cell suspension using collagenase II (600 U/mL) and DNase I (60 U/mL) as we previously described [14]. Cells were incubated at 37 °C with 5 % CO_2 and cultured in complete DMEM/F12 media (supplemented with 10 % FBS and 1 % antibiotics/antimicotics) until passage 2 (P2).

2.10. Migration assay

Cardiac fibroblasts were plated in an Electric Cell-substrate Impedance Sensing (#ECIS-1600R, Applied Biophysics®) and allowed to proliferate until confluence. An electric wound (1400uA, 60,000 Hz, 20 s) was induced and the wells were rinsed to remove dead cells. The media was replaced with serum free media (SFM, negative control) ± p1159 (100 nM or 500 nM). Complete media was used as positive control ($n = 6$/group). Cell migration was recorded in real time for 48 h. For the experiments testing integrin alpha 4 (Itgα4) as the receptor for p1159, cardiac fibroblasts were cultured in SFM with Itgα4 blocking antibody (#NBP1-26661, Novus Biologicals; Itgα4i) 15 μg/mL for 2 h before wound induction, followed by treatment as listed in Table 1.

Table 1
Treatments and respective control groups.

Treatment groups	Media components
Negative control	SFM
Positive control	10 % FBS
Itgα4i negative control	SFM + Itgα4i
Itgα4i positive control	10 % FBS + Itgα4i
100 nM p1159	SFM + 100 nM p1159
500 nM p1159	SFM + 500 nM p1159
100 nM p1159 + Itgα4i	SFM + 100 nM p1159 + Itgα4i
500 nM p1159 + Itgα4i	SFM + 500 nM p1159 + Itgα4i

SFM = serum free media, FBS = fetal bovine serum, Itgα4i = integrin alpha 4 blocking antibody.

2.11. Human cardiac fibroblasts culture and stimulation

To validate our findings across species, we cultured human cardiac fibroblasts isolated from ventricles of adult heart (HCF, PromoCell # C-12377) in fibroblast growth medium 3 (PromoCell) until P5. Confluent cells were starved overnight in SFM and incubated with p1159 as described above (Table 1). After incubation, cells were rinsed and either fixed for immunofluorescence or lysed for protein and/or RNA extraction. Protein lysates were obtained with 1× ice cold lysis buffer with 1× protease inhibitors (Abcam, ab152163), according to manufacturer's instructions and quantified for immunoblotting.

2.12. Cell motility, RNA extraction, quantification and gene array

Gene arrays for mouse cell motility (#PAMM-128ZE, Qiagen) and ECM, cell adhesion molecules, and receptors (#PAMM-013, Qiagen) were used to determine p1159 dependent effects on both fibroblast migration and ECM expression. Threshold cycle (Ct) values were normalized by the internal control genes Actb, Gapdh, and Hsp90ab1, and final measurements were converted into $2^{-\Delta Ct}$ to get the expression fold change versus negative control.

2.13. Rho activation

Fibroblasts were cultured on sterile coverslips in 24-well plates until cells reached 60 % confluence. The cells were starved overnight in low serum media (LSM; DMEM/F12 with 0.5 % FBS). The treatment groups listed on Table 1 were tested in triplicates and incubated for 3, 5, and 15 min to measure the stimulation of Rho activation by p1159 ± Itgα4i. After each incubation, cells were fixed in 100 % ethanol for 20 min and air dried. Cells were incubated overnight with primary antibodies against Itgα4 (Cell Signaling) and anti-RhoA mouse IgM Mab (Cytoskeleton). The next day, appropriate secondary antibodies, conjugated with Alexa Fluor dyes were used at room temperature for 1 h to optimize visual detection. Coverlips were mounted with Vectashield DAPI (Vector) medium and images were captured using an Olympus IMT-2 fluorescent microscope under the same exposure conditions.

2.14. Co-localization of p1159 and Itgα4

HCF were seeded in slides and stimulated with different doses of a FITC-labeled p1159 ± Itgα4i as described above. Cells were fixed and processed for immunofluorescence staining against Itgα4. Single plane images were collected using the Zeiss LSM 800 laser scanning confocal microscope and analyzed with ZEN Blue 2012 software.

2.15. Statistical analysis

Power analysis was used to determine group sizes (GraphPad StatMate 2) based on previous data from our lab and others. Data are reported as mean ± SEM and outliers were identified using the Grubbs method with an alpha set at 0.05 [21]. Outliers were included when it did not affect the final statistical result; when the outlier affected overall results, this was noted on the results section and the final statistical analysis was presented with and without the outlier. Comparisons between groups were performed using unpaired *t*-test or Mann-Whitney test when comparing two groups (e.g., immunoblots), one-way ANOVA when comparing 3 groups or more followed by the Tukey post hoc test when the Bartlett's variation test passed or using the nonparametric Kruskal-Wallis test followed by Dunn post hoc test when the Bartlett's variation test did not pass (e.g., mRNA analysis), and two-way ANOVA followed by the Bonferroni's multiple comparisons test when two independent variables were being tested across groups (e.g., echocardiography parameters). Survival analysis was performed using

the Kaplan-Meier (nonparametric) method. A $p < 0.05$ was considered significant (GraphPad Prism 9).

3. Results

Figures display aggregate data from both sexes, sex-specific data can be found in the supplemental data.

3.1. p1159 long-term treatment improves cardiac function post-MI

Infarct sizes were measured both at D7 and D28 by serial echocardiography using strain analysis following manufacturer's instructions. At D7, infarct size did not differ between saline and p1159-treated animals. Interestingly, while infarct size in the vehicle control group had a significant increase with time, mice treated with p1159 did not show an increase in infarct size (Fig. 1A), suggesting that peptide treatment attenuates the expansion of the infarcted scar. This effect could be a result of reduced adverse remodeling and/or increased vessel reperfusion. Of note, survival rates between treatments did not show significant differences (Fig. 1B, saline 68 % versus p1159 83 %).

Serial echocardiography of mice treated with p1159, vehicle control, and surgical controls (sham) were acquired before (baseline) and after surgery every seven days (3 h, D7, D14, D21, and D28) to evaluate the evolution of cardiac parameters and function post-MI (Fig. 1C and Table 2). As expected, all systolic parameters measured were different between post-MI treatment groups and sham. Systolic function, as measured by ejection fraction (EF), was significantly improved at D14, D21, and D28 in the p1159-treated mice compared to saline controls (Fig. 1D, D28 saline EF = 14 ± 7, D28 p1159 EF = 28 ± 14, and Supplemental Fig. S1A).

The preload and afterload capacities of the LV were examined respectively by end-diastolic (EDV) and end-systolic volumes (ESV) to evaluate how p1159 treatment affects the LV integrity after ischemic injury. Long-term p1159 therapy reduced LV dilation, as seen by decreased EDV and ESV, compared to vehicle control, since D7 until the end of the treatment (Fig. 1E–F). While both sexes showed reduced dilation with peptide treatment, these differences were observed earlier in males (Supplemental Fig. S1B–C).

Given that increased ESV can be an indicator for a larger infarcted area [22], these data are consistent with our measurements of infarct size as shown in Fig. 1A. Stroke volume (SV) only differed between groups at D28, and this difference was driven by females (Table 2 A–C). In addition, the LV interior diameters during diastole (LVIDd) and systole (LVIDs) were calculated to analyze the LV dimension in the cardiac cycle. Changes in LV dimensions were found between groups after D7 post-MI, with p1159 treatment attenuating the expansion of LV diameter compared to vehicle (Fig. 1G–H). These changes were temporally distinct in males and females and more marked in males, indicating sex

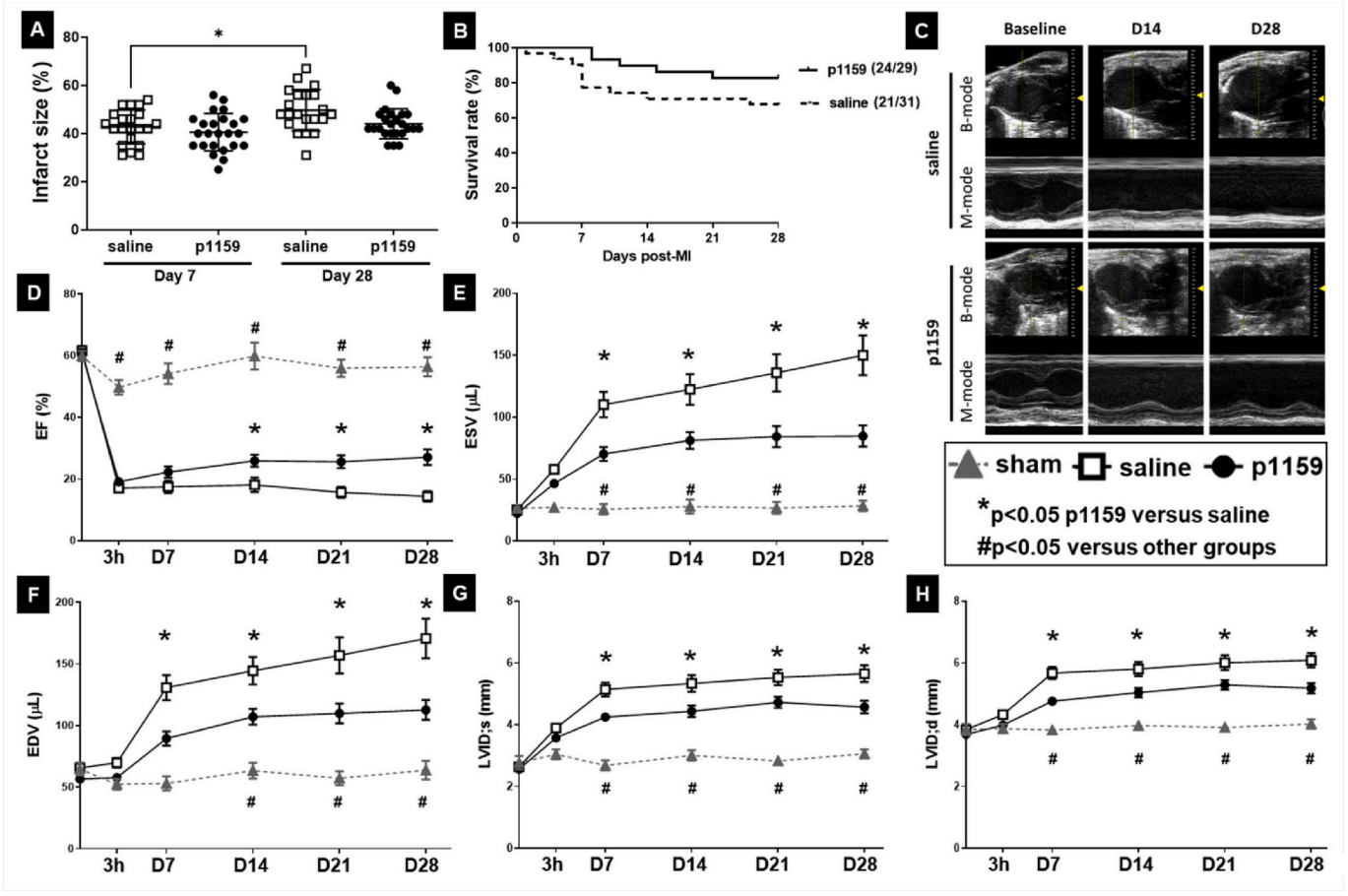

Fig. 1. Long term treatment with p1159 improved cardiac function post-MI. A. Infarct Size at D7 and D-28. While the saline group showed a significant increase in infarct size with time (D7 to D28), p1159-treated animals maintained the same percentage of infarct size throughout the study. Infarct size measured by strain analysis using echocardiography (*$p < 0.05$). B. Survival curves post-MI. Mortality rate post-MI did not differ between treatment groups. C. Representative images of serial echocardiography (baseline, D14, and D28) post-MI of mice treated with p1159 or vehicle control (saline) in B- and M-mode of long-axis view. D. After D14, p1159 treated animals display improved systolic function. Compared to controls, ejection fraction (EF) increased in p1159 treated mice at D14 to D28. E–H. p1159 attenuates eccentric remodeling post-MI by decreasing LV dilation. Compared to saline control, end-systolic (ESV) and end-diastolic volumes (EDV) decreased in peptide treated mice (D7 to D28). Similarly, the LV interior diameter in diastole (LVIDd) and systole (LVIDs) were decreased in p1159 mice compared to vehicle. *$p < 0.05$ versus same day peptide; #$p < 0.05$ versus same day saline and p1159. $n = 5$ sham, $n = 21$–24 animals/group.

Table 2
p1159 treatment blunts cardiac dysfunction post-MI. Echocardiographic parameters quantified serially across both sexes (A), males (B) and females (C). Values are mean ± SEM.

(A) Both sexes	SHAM						Saline						p1159					
	Days post-MI						Days post-MI						Days post-MI					
	Baseline	3 h	D7	D14	D21	D28	Baseline	3 h	D7	D14	D21	D28	Baseline	3 h	D7	D14	D21	D28
Body weight (g)	27 ± 4.8	n/a	n/a	n/a	n/a	27 ± 4.1	29 ± 4.6	n/a	n/a	n/a	n/a	28 ± 4.0	28 ± 4.9	n/a	n/a	n/a	n/a	28 ± 4.3
LV mass (mg)	n/a	n/a	n/a	n/a	n/a	107 ± 20.6	n/a	n/a	n/a	n/a	n/a	146 ± 31.1	n/a	n/a	n/a	n/a	n/a	128 ± 28.0
Heart rate (BPM)	441 ± 22	399 ± 60	477 ± 63	453 ± 42	487 ± 60	472 ± 40	432 ± 25	406 ± 76	485 ± 64*	479 ± 50*	488 ± 51*	474 ± 48	439 ± 33	402 ± 50	474 ± 49	477 ± 44	454 ± 46	458 ± 39
ESV (μl)	27 ± 9	27 ± 10	26 ± 13	28 ± 19	27 ± 16	28 ± 14	25 ± 8	58 ± 16*	110 ± 45*,+	123 ± 57*,+	136 ± 69*,+	150 ± 74*,+	23 ± 8	47 ± 13*	70 ± 28*,+,#	81 ± 33*,+,#	84 ± 39*,+,#	85 ± 42*,+,#
EDV (μl)	65 ± 18	53 ± 14	53 ± 18	64 ± 21	57 ± 19	64 ± 25	66 ± 16	70 ± 18*	131 ± 44*,+	144 ± 51*,+	157 ± 67*,+	171 ± 74*,+	57 ± 15	58 ± 16	89 ± 28*,#	107 ± 32*,+,#	110 ± 37*,+,#	113 ± 39*,+,#
SV (μL)	38 ± 9	25 ± 5*	28 ± 6*	36 ± 6	31 ± 5	36 ± 14	40 ± 10	12 ± 4*,+	21 ± 8*	22 ± 9*,+	21 ± 7*,+	21 ± 7*,+	34 ± 9	11 ± 5*,+	19 ± 7*	26 ± 8+	25 ± 7	28 ± 10#
EF (%)	60 ± 6	50 ± 7	54 ± 11	60 ± 14	56 ± 9	56 ± 10	62 ± 7	17 ± 4*,+	17 ± 9*,+	18 ± 11*,+	16 ± 8*,+	14 ± 8*,+	61 ± 7	19 ± 6*,+	22 ± 9*,+	26 ± 9*,+,#	26 ± 10*,+,#	27 ± 12*,+,#
LVAWd (mm)	0.90 ± 0.11	0.99 ± 0.20	1.07 ± 0.09*	1.01 ± 0.10	0.93 ± 0.14	1.0 ± 0.16	0.89 ± 0.12	0.79 ± 0.18	0.67 ± 0.23+	0.55 ± 0.17*,+	0.59 ± 0.21*,+	0.45 ± 0.22*,+	0.89 ± 0.14	0.86 ± 0.15	0.69 ± 0.24+	0.61 ± 0.24*,+	0.61 ± 0.24*,+	0.55 ± 0.25*,+
LVAWs (mm)	1.18 ± 0.19	1.23 ± 0.19	1.37 ± 0.15	1.28 ± 0.14	1.26 ± 0.19	1.25 ± 0.17	1.21 ± 0.15	0.88 ± 0.20	0.77 ± 0.26*	0.62 ± 0.22*,+	0.63 ± 0.22*	0.51 ± 0.27*,+	1.25 ± 0.21	0.90 ± 0.16*,+	0.75 ± 0.28*,+	0.70 ± 0.31*,+	0.68 ± 0.31*,+	0.63 ± 0.35*,+
LVIDd; EDD (mm)	3.85 ± 0.60	3.88 ± 0.48	3.84 ± 0.37	3.98 ± 0.46	3.92 ± 0.40	4.03 ± 0.50	3.85 ± 0.46	4.33 ± 0.56	5.68 ± 0.85*,+	5.81 ± 1.04*,+	6.01 ± 1.12*,+	6.10 ± 1.06*,+	3.69 ± 0.60	4.00 ± 0.43	4.77 ± 0.60*,+,#	5.05 ± 0.73*,+,#	5.30 ± 0.71*,+,#	5.19 ± 0.82*,+,#
LVIDs; ESD (mm)	2.78 ± 0.73	3.05 ± 0.51	2.69 ± 0.52	3.01 ± 0.56	2.84 ± 0.44	3.07 ± 0.48	2.65 ± 0.51	3.90 ± 0.57*	5.15 ± 0.97*,+	5.34 ± 1.24*,+	5.54 ± 1.16*,+	5.66 ± 1.24*,+	2.57 ± 0.62	3.58 ± 0.43*	4.26 ± 0.68*,+,#	4.44 ± 0.91*,+,#	4.73 ± 0.83*,+,#	4.58 ± 1.00*,+,#
LVPWd (mm)	1.03 ± 0.24	0.86 ± 0.16	1.05 ± 0.19	1.14 ± 0.15	1.01 ± 0.14	1.00 ± 0.13	1.08 ± 0.21	0.81 ± 0.16	0.86 ± 0.27	1.01 ± 0.36	0.94 ± 0.29	0.87 ± 0.37*	1.02 ± 0.19	0.82 ± 0.15*	0.91 ± 0.29	0.95 ± 0.32	0.87 ± 0.26	1.02 ± 0.30
LVPWs (mm)	1.25 ± 0.19	1.07 ± 0.24	1.30 ± 0.23	1.30 ± 0.22	1.26 ± 0.12	1.19 ± 0.17	1.33 ± 0.19	0.91 ± 0.20*	1.03 ± 0.31	1.17 ± 0.39	1.09 ± 0.28	0.99 ± 0.42*	1.28 ± 0.19	0.95 ± 0.20*	1.04 ± 0.39	1.11 ± 0.36	1.03 ± 0.27	1.18 ± 0.35
FS SAX (%)	29.1 ± 9.6	21.7 ± 5.3	30.3 ± 8.3	24.8 ± 7.8	27.9 ± 4.3	24.1 ± 5.5	31.8 ± 7.8	10.0 ± 4.7*	9.8 ± 5.1*,+	9.3 ± 6.8*,+	8.3 ± 3.8*,+	8.3 ± 5.1*,+	31.3 ± 7.5	10.4 ± 4.1*	11.0 ± 5.2*,+	12.6 ± 7.4*,+	11.0 ± 4.8*,+	13.0 ± 6.3*,+
Cardiac output (mL/min)	17 ± 4	10 ± 3*	13 ± 3	16 ± 3	15 ± 2	17 ± 7	17 ± 5	5 ± 3*,+	10 ± 4*	10 ± 4*,+	10 ± 3*,+	10 ± 3*,+	15 ± 4	5 ± 2*,+	9 ± 3*	12 ± 4	11 ± 3	13 ± 5+
LV mass/BW (mg/g)	n/a	n/a	n/a	n/a	n/a	4.11 ± 0.61	n/a	n/a	n/a	n/a	n/a	5.25 ± 0.98	n/a	n/a	n/a	n/a	n/a	4.59 ± 0.77#
RV mass/BW (mg/g)	n/a	n/a	n/a	n/a	n/a	0.73 ± 0.14	n/a	n/a	n/a	n/a	n/a	1.07 ± 0.43	n/a	n/a	n/a	n/a	n/a	0.91 ± 0.27
Tibia length (mm)	n/a	n/a	n/a	n/a	n/a	17.45 ± 0.4	n/a	n/a	n/a	n/a	n/a	17.56 ± 0.4	n/a	n/a	n/a	n/a	n/a	17.29 ± 0.4
Lung W/D weight ratio (mg)	n/a	n/a	n/a	n/a	n/a	4.35 ± 0.7	n/a	n/a	n/a	n/a	n/a	4.26 ± 0.6	n/a	n/a	n/a	n/a	n/a	4.35 ± 0.5
Number of samples	11	11	11	11	11	11	21	21	21	21	21	21	24	24	24	24	24	24

(B) Males	SHAM						Saline						p1159					
	Days post-MI						Days post-MI						Days post-MI					
	Baseline	3 h	D7	D14	D21	D28	Baseline	3 h	D7	D14	D21	D28	Baseline	3 h	D7	D14	D21	D28
Body weight (g)	31 ± 1.1	n/a	n/a	n/a	n/a	30 ± 1.9	32 ± 2.9	n/a	n/a	n/a	n/a	31 ± 1.8	33 ± 3.7	n/a	n/a	n/a	n/a	32 ± 2.3
LV mass (mg)	n/a	n/a	n/a	n/a	n/a	119 ± 22.4	n/a	n/a	n/a	n/a	n/a	167 ± 32.1	n/a	n/a	n/a	n/a	n/a	149 ± 29.4
Heart rate (BPM)	455 ± 17	418 ± 69	450 ± 57	431 ± 33	453 ± 27	485 ± 44	429 ± 27	405 ± 88	501 ± 77	474 ± 64	485 ± 59	480 ± 54	441 ± 43	392 ± 54	454 ± 45	478 ± 60	447 ± 51	448 ± 38
ESV (μl)	33 ± 7	33 ± 8	35 ± 10	41 ± 20	36 ± 20	36 ± 18	30 ± 7	64 ± 17*	121 ± 57*,+	135 ± 69*,+	149 ± 82*,+	164 ± 87*	28 ± 7	56 ± 13*	84 ± 28*	89 ± 29*	86 ± 33*	86 ± 33*,#
EDV (μl)	77 ± 12	60 ± 8	67 ± 13	80 ± 20	71 ± 21	78 ± 31	74 ± 17	75 ± 18*	145 ± 54*,+	157 ± 60*,+	172 ± 81*,+	187 ± 86*,+	68 ± 13	68 ± 17	106 ± 28*	117 ± 28*	115 ± 34*	115 ± 37*,#
SV (μL)	44 ± 6	27 ± 3*	31 ± 4	38 ± 6	35 ± 3	48 ± 17	44 ± 12	11 ± 4*,+	24 ± 9*	23 ± 10*,+	24 ± 8*	23 ± 6*	40 ± 9	12 ± 7*,+	22 ± 8*	28 ± 7*	29 ± 6	29 ± 11
EF (%)	57 ± 4	45 ± 7	47 ± 4	50 ± 14	52 ± 11	55 ± 12	60 ± 5	15 ± 4*,+	19 ± 11*,+	18 ± 12*,+	17 ± 10*,+	15 ± 9*,+	59 ± 8	17 ± 8*,+	22 ± 9*,+	25 ± 9*,+	27 ± 10*,+	25 ± 9*,+
LVAWd (mm)	0.89 ± 0.09	1.04 ± 0.28	1.06 ± 0.06	1.02 ± 0.10	0.94 ± 0.12	0.97 ± 0.15	0.91 ± 0.10	0.79 ± 0.23	0.71 ± 0.27	0.61 ± 0.16*,+	0.65 ± 0.20*	0.54 ± 0.27*,+	0.98 ± 0.12	0.84 ± 0.11	0.75 ± 0.21	0.63 ± 0.32+	0.65 ± 0.25	0.65 ± 0.26
LVAWs (mm)	1.13 ± 0.10	1.23 ± 0.27	1.34 ± 0.10	1.23 ± 0.16	1.24 ± 0.26	1.26 ± 0.14	1.24 ± 0.10	0.89 ± 0.26*	0.84 ± 0.31*,+	0.69 ± 0.24*,+	0.70 ± 0.21*,+	0.61 ± 0.34*,+	1.36 ± 0.16	0.88 ± 0.17*	0.82 ± 0.21*,+	0.75 ± 0.37*,+	0.74 ± 0.35*,+	0.76 ± 0.37*,+
LVIDd; EDD (mm)	4.31 ± 0.04	4.13 ± 0.28	4.10 ± 0.39	4.30 ± 0.46	4.19 ± 4.3	4.27 ± 0.60	3.92 ± 0.51	4.41 ± 0.62	5.94 ± 0.99*,+	6.00 ± 1.34*,+	6.30 ± 1.20*,+	6.29 ± 1.16*,+	3.89 ± 0.60	4.28 ± 0.34	4.99 ± 0.49*	5.08 ± 0.64*	5.25 ± 0.80*	5.22 ± 0.86*
LVIDs; ESD (mm)	3.34 ± 0.11	3.35 ± 0.39	3.03 ± 0.54	3.36 ± 0.45	3.12 ± 0.47	3.15 ± 0.67	2.73 ± 0.48	3.96 ± 0.69*	5.39 ± 1.17*,+	5.49 ± 1.66*,+	5.79 ± 1.26*,+	5.88 ± 1.48*,+	2.73 ± 0.67	3.84 ± 0.32	4.46 ± 0.53*	4.45 ± 0.76*	4.59 ± 0.87*	4.54 ± 1.06*,#
LVPWd (mm)	0.97 ± 0.15	0.87 ± 0.13	1.00 ± 0.15	1.05 ± 0.16	1.05 ± 0.14	0.98 ± 0.10	1.18 ± 0.18	0.81 ± 0.19	0.91 ± 0.18	0.96 ± 0.42	0.94 ± 0.26	0.79 ± 0.44*	1.10 ± 0.15	0.82 ± 0.15*	0.99 ± 0.22	1.15 ± 0.28+	1.00 ± 0.19	1.02 ± 0.19
LVPWs (mm)	1.23 ± 0.13	1.09 ± 0.19	1.20 ± 0.18	1.22 ± 0.15	1.28 ± 0.14	1.26 ± 0.16	1.42 ± 0.15	0.91 ± 0.17*	1.10 ± 0.18	1.14 ± 0.51	1.09 ± 0.29	0.87 ± 0.49*	1.40 ± 0.18	0.94 ± 0.22*	1.11 ± 0.23	1.31 ± 0.28+	1.15 ± 0.18	1.21 ± 0.28
FS SAx (%)	22.6 ± 2.4	19.1 ± 4.8	26.5 ± 6.6	22.0 ± 3.0	25.9 ± 3.8	26.6 ± 6.1	30.6 ± 6.1*	10.5 ± 6.1*	10.0 ± 6.0*,+	11.2 ± 8.9*,+	8.5 ± 4.1*,+	8.5 ± 6.6*,+	30.7 ± 9.3	10.2 ± 4.6*	10.6 ± 3.8*,+	12.8 ± 6.4*	13.1 ± 4.2*,+	13.9 ± 8.1*,+
Cardiac output (mL/min)	20 ± 3	11 ± 3*	14 ± 3	17 ± 4	16 ± 2	20 ± 9	19 ± 5	4 ± 1*,+	12 ± 5*	10 ± 4*	11 ± 3*	11 ± 3*,+	18 ± 5	5 ± 2*	10 ± 3*	14 ± 4	13 ± 2	13 ± 5#
LV mass/BW (mg/g)	n/a	n/a	n/a	n/a	n/a	3.93 ± 0.52	n/a	n/a	n/a	n/a	n/a	5.37 ± 1.11	n/a	n/a	n/a	n/a	n/a	4.60 ± 0.78
RV mass/BW (mg/g)	n/a	n/a	n/a	n/a	n/a	0.72 ± 0.19	n/a	n/a	n/a	n/a	n/a	0.93 ± 0.32	n/a	n/a	n/a	n/a	n/a	0.87 ± 0.23
Tibia length (mm)	n/a	n/a	n/a	n/a	n/a	17.45 ± 0.5	n/a	n/a	n/a	n/a	n/a	17.66 ± 0.3	n/a	n/a	n/a	n/a	n/a	17.43 ± 0.6
Lung W/D weight ratio (mg)	n/a	n/a	n/a	n/a	n/a	4.30 ± 0.5	n/a	n/a	n/a	n/a	n/a	4.00 ± 0.6	n/a	n/a	n/a	n/a	n/a	4.12 ± 0.3
Number of samples	5	5	5	5	5	5	10	10	10	10	10	10	10	10	10	10	10	10

(C) Females	SHAM						Saline						p1159					
	Days post-MI						Days post-MI						Days post-MI					
	Baseline	3 h	D7	D14	D21	D28	Baseline	3 h	D7	D14	D21	D28	Baseline	3 h	D7	D14	D21	D28
Body weight (g)	23 ± 2.1	n/a	n/a	n/a	n/a	24 ± 2.3	26 ± 3.7	n/a	n/a	n/a	n/a	25 ± 2.9	25 ± 2.0	n/a	n/a	n/a	n/a	25 ± 2.2
LV mass (mg)	n/a	n/a	n/a	n/a	n/a	96 ± 12.2	n/a	n/a	n/a	n/a	n/a	127 ± 12.5	n/a	n/a	n/a	n/a	n/a	113 ± 14.5

(*continued on next page*)

Table 2 (*continued*)

(C) Females	SHAM						Saline						p1159					
	Days post-MI						Days post-MI						Days post-MI					
	Baseline	3 h	D7	D14	D21	D28	Baseline	3 h	D7	D14	D21	D28	Baseline	3 h	D7	D14	D21	D28
Heart rate (BPM)	430 ± 21	379 ± 48	494 ± 65	471 ± 42	515 ± 68	461 ± 37	434 ± 23	406 ± 67	466 ± 43	484 ± 36^{+}	491 ± 46^{+}	468 ± 43	437 ± 26	409 ± 48	489 ± 49$^{*,+}$	477 ± 31^{+}	460 ± 42^{+}	464 ± 40^{+}
ESV (μl)	21 ± 8	21 ± 9	19 ± 12	16 ± 7	19 ± 4	22 ± 7	22 ± 7	53 ± 13	98 ± 25$^{*,+}$	112 ± 44$^{*,+}$	125 ± 55$^{*,+}$	137 ± 62$^{*,+}$	19 ± 7	41 ± 9	61 ± 24*	76 ± 36$^{*,+}$	83 ± 45$^{*,+}$	84 ± 49$^{*,+,\#}$
EDV (μl)	55 ± 15	45 ± 16	44 ± 16	50 ± 8	46 ± 4	53 ± 11	58 ± 12	66 ± 17*	116 ± 24$^{*,+}$	133 ± 41$^{*,+}$	143 ± 52$^{*,+}$	156 ± 61$^{*,+}$	49 ± 12	51 ± 12	77 ± 22*	100 ± 33$^{*,+}$	105 ± 40$^{*,+}$	111 ± 42$^{*,+,\#}$
SV (μL)	33 ± 8	24 ± 7	25 ± 7	34 ± 5	27 ± 3	30 ± 7	37 ± 8	13 ± 5$^{*,+}$	17 ± 6*	21 ± 8^{+}	18 ± 5*	18 ± 8$^{*,+}$	30 ± 6	11 ± 4$^{*,+}$	17 ± 5*	24 ± 8^{+}	22 ± 6*	27 ± 9$^{\#}$
EF (%)	62 ± 6	55 ± 3	59 ± 12	68 ± 9	59 ± 7	58 ± 9	64 ± 8	19 ± 4$^{*,+}$	16 ± 6$^{*,+}$	18 ± 9$^{*,+}$	14 ± 6$^{*,+}$	14 ± 7$^{*,+}$	62 ± 6	20 ± 4$^{*,+}$	23 ± 9$^{*,+}$	26 ± 10$^{*,+}$	25 ± 10$^{*,+}$	28 ± 14$^{*,+,\#}$
LVAWd (mm)	0.90 ± 0.14	0.94 ± 0.08	1.07 ± 0.12	1.01 ± 0.11	0.91 ± 0.17	1.02 ± 0.18	0.86 ± 0.13	0.79 ± 0.14	0.63 ± 0.18^{+}	0.49 ± 0.17$^{*,+}$	0.53 ± 0.20$^{*,+}$	0.36 ± 0.12$^{*,+}$	0.83 ± 0.12	0.87 ± 0.17	0.64 ± 0.26^{+}	0.59 ± 0.18^{+}	0.58 ± 0.23^{+}	0.48 ± 0.23$^{*,+}$
LVAWs (mm)	1.22 ± 0.24	1.23 ± 0.09	1.39 ± 0.19	1.32 ± 0.11	1.27 ± 0.14	1.24 ± 0.20	1.18 ± 0.19	0.87 ± 0.15*	0.70 ± 0.19$^{*,+}$	0.56 ± 0.19$^{*,+}$	0.57 ± 0.23$^{*,+}$	0.42 ± 0.14$^{*,+}$	1.17 ± 0.20	0.91 ± 0.16	0.69 ± 0.32$^{*,+}$	0.66 ± 0.27$^{*,+}$	0.63 ± 0.28$^{*,+}$	0.53 ± 0.31$^{*,+}$
LVIDd; EDD (mm)	3.47 ± 0.58	3.63 ± 0.53	3.66 ± 0.26	3.71 ± 0.26	3.70 ± 0.21	3.84 ± 0.32	3.79 ± 0.41	4.26 ± 0.52	5.39 ± 0.58$^{*,+}$	5.64 ± 0.70$^{*,+}$	5.76 ± 1.02$^{*,+}$	5.92 ± 0.97$^{*,+}$	3.55 ± 0.59	3.81 ± 0.39	4.61 ± 0.64*	5.02 ± 0.81$^{*,+}$	5.33 ± 0.66$^{*,+}$	5.16 ± 0.82$^{*,+}$
LVIDs; ESD (mm)	2.32 ± 0.71	2.75 ± 0.46	2.46 ± 0.40	2.72 ± 0.49	2.61 ± 0.27	2.99 ± 0.32	2.57 ± 0.54	3.85 ± 0.47*	4.88 ± 0.66$^{*,+}$	5.21 ± 0.75$^{*,+}$	5.31 ± 1.07$^{*,+}$	5.46 ± 1.01$^{*,+}$	2.45 ± 0.57	3.41 ± 0.42*	4.11 ± 0.75$^{*,+}$	4.44 ± 1.04$^{*,+}$	4.86 ± 0.80$^{*,+}$	4.60 ± 0.99$^{*,+}$
LVPWd (mm)	1.08 ± 0.30	0.85 ± 0.20	1.08 ± 0.22	1.21 ± 0.11	0.97 ± 0.14	1.03 ± 0.15	0.98 ± 0.20	0.81 ± 0.14	0.80 ± 0.34	1.06 ± 0.30	0.94 ± 0.32	0.94 ± 0.30	0.96 ± 0.20	0.82 ± 0.16	0.86 ± 0.32	0.81 ± 0.28^{+}	0.76 ± 0.26	1.02 ± 0.37
LVPWs (mm)	1.26 ± 0.25	1.05 ± 0.30	1.36 ± 0.25	1.36 ± 0.25	1.25 ± 0.10	1.13 ± 0.16	1.26 ± 0.20	0.92 ± 0.24	0.96 ± 0.42	1.19 ± 0.28	1.09 ± 0.29	1.10 ± 0.34	1.20 ± 0.17	0.95 ± 0.20	0.98 ± 0.47	0.96 ± 0.34	0.91 ± 0.29	1.16 ± 0.40
FS SAx (%)	34.5 ± 10.1	24.4 ± 4.8	32.9 ± 8.9	27.1 ± 10.1	29.6 ± 4.2	22.0 ± 4.5	32.8 ± 9.3	9.6 ± 4.0$^{*,+}$	9.6 ± 4.1$^{*,+}$	7.8 ± 4.4$^{*,+}$	8.2 ± 3.6$^{*,+}$	8.1 ± 3.8$^{*,+}$	31.6 ± 6.2	10.5 ± 4.0$^{*,+}$	11.3 ± 6.2$^{*,+}$	12.5 ± 8.4$^{*,+}$	9.2 ± 4.8$^{*,+}$	11.4 ± 5.5$^{*,+}$
Cardiac output (mL/min)	14 ± 4	9 ± 2	12 ± 4	16 ± 3	14 ± 2	14 ± 4	16 ± 4	6 ± 3*	8 ± 3*	10 ± 3$^{*,+}$	9 ± 3$^{*,+}$	8 ± 3$^{*,+}$	13 ± 2	4 ± 2*	8 ± 3*	12 ± 4	10 ± 3	12 ± 4$^{\#}$
LV mass/BW (mg/g)	n/a	n/a	n/a	n/a	n/a	4.26 ± 0.69	n/a	n/a	n/a	n/a	n/a	5.14 ± 0.89	n/a	n/a	n/a	n/a	n/a	4.58 ± 0.78
RV mass/BW (mg/g)	n/a	n/a	n/a	n/a	n/a	0.73 ± 0.09	n/a	n/a	n/a	n/a	n/a	1.19 ± 0.49	n/a	n/a	n/a	n/a	n/a	0.94 ± 0.29
Tibia length (mm)	n/a	n/a	n/a	n/a	n/a	17.45 ± 0.4	n/a	n/a	n/a	n/a	n/a	17.47 ± 0.5	n/a	n/a	n/a	n/a	n/a	17.19 ± 0.3
Lung W/D weight ratio (mg)	n/a	n/a	n/a	n/a	n/a	4.40 ± 0.9	n/a	n/a	n/a	n/a	n/a	4.22 ± 0.6	n/a	n/a	n/a	n/a	n/a	4.52 ± 0.6
Number of samples	6	6	6	6	6	6	11	11	11	11	11	11	14	14	14	14	14	14

* $p < 0.05$ against respective baseline.
$^{+}$ $p < 0.05$ against same day sham.
$^{\#}$ $p < 0.05$ against same day saline.

specificity in LV structural composition throughout time (supplemental Fig. S1D–E). Of note, we did not observe differences in wall thicknesses between groups.

Our data did not show treatment dependent sex-differences in most parameters measured. Nonetheless, peptide treatment blunted LV dilation to a higher extent in males (D7 to D28 EDV, ESV, LVIDd, and LVIDs sham vs peptide p = NS) than in females (EDV, ESV, LVIDd, and LVIDs $p < 0.05$ sham vs saline, Table 2). Several studies have reported sex differences in MI occurrence and progression to HF [23]; nevertheless, no significant sex differences have been reported on incidence of LV remodeling post-MI [24]. It is possible that p1159 treatment has blunted some sex differences; however, further studies using hormonal manipulation and/or older animals will be necessary to examine peptide effects on sex-differences post-MI.

3.2. p1159 promoted fiber alignment in the infarcted area

We examined whether p1159 therapy affects the long-term levels of collagen and the distribution and alignment of the collagen fibers, both in the infarct and border zone post-MI. Infarcted LVs were stained with picrosirius red to identify, quantify, and determine the orientation of collagen fibers. When we analyzed the combined data from both sexes, collagen levels from the border zone of vehicle control and p1159-treated mice did not differ with time or between groups. The infarct zone of p1159-treated mice showed an increase in collagen levels at D14 compared to saline, but this difference was not present at D28 (Fig. 2A). Moreover, this effect was absent in the individual analysis of males and females (supplemental Fig. S2). Importantly, collagen levels did not continue to rise and no changes, either between groups or time-points, were observed at D28. It is possible that increased fibroblast migration during early remodeling accelerates collagen deposition by D14 stabilizing the scar earlier. An earlier stable scar could explain the improved EF and reduced dilation observed with peptide treatment. To determine whether there were differences in the scar structure we analyzed scar fiber alignment. Using a birefringence filter, the LV images stained with PSR were digitally subtracted to isolate the collagen fibers from the remaining tissue. All samples were normalized by their respective LV circumferential section, i.e. pericardium = 0°, before identifying the probability (percentage) of collagen fiber direction in 10 degree increments (from −90° to +90°) using a previously reported MATLAB algorithm [19]. As expected, collagen fiber orientation displayed higher variation between treatments at D7; since at this time collagen is still being secreted and granulation tissue is present [25]. While control LVs showed higher numbers of fibers aligned at +20° to +40° in the border zone, fibers in peptide treated mice aligned mostly at −20° to +10°, with a significant higher number of fibers aligned at −10° compared to D7 controls (Fig. 2B). With time, fibers in the border zone aligned parallel to the epicardium, with the highest probabilities between −20° and +20°, independent of treatment. In contrast, the infarct zone of p1159-treated mice at most time-points presented increased numbers of fibers with angles close to 0° (D14 fibers at 10° $p < 0.05$ p1159 versus saline group). In a circumferential section of LV, a 0° angle means the fiber is parallel to the epicardium. In contrast, at the end of the study (D28) the control group showed significantly increased number of fibers perpendicular to the pericardium (−90°, −80°, and 90°) in the infarcted area.

3.3. Protein expression and ECM composition

The quality of the infarct scar together with the rate of wound healing are determinants of how cardiac remodeling modulates ECM protein synthesis and degradation according to the hemodynamic load, which determines LV functionality [26]. Herein, we investigated how p1159 long-term treatment is involved in ECM metabolism post-MI, by measuring the levels of ECM proteins directly related to formation of the infarcted scar. We started by determining levels of fibrillar collagen. Levels of collagen type I were similar between p1159-treated mice and vehicle controls at D28 in both sexes (Fig. 2C). Notably, collagen type III was increased in the infarct zone of mice treated with p1159 compared to saline control, in addition to a decrease in its fragmentation (Fig. 2C, top mid panels). We also quantified protein expression of osteopontin, decorin, periostin, and lysyl oxidase. Osteopontin is an ECM glycoprotein that it is highly expressed by fibroblasts and macrophages post-MI, and exaggerated levels have been associated with cardiac fibrosis and systolic dysfunction [27]. Decorin is involved in the fibrillogenesis of collagens, and it plays a role in the appropriate assembly of ECM post-MI [28]. Likewise, periostin is necessary for cardiac healing post-MI since it promotes assembly and collagen fibril formation [29,30]. Our data show the levels of osteopontin, decorin and periostin from the infarcted LV of mice treated ± p1159 were similar, indicating that this matricryptin does not appear to regulate these ECM molecules post-MI. Nonetheless, lysyl oxidase (LOX2) was significantly decreased in female mice treated with p1159, but not in males (Fig. 2C, bottom right panels). LOX2 increases the collagen fiber cross-links post-MI [31] and exaggerated levels would thus increase stiffness of the cardiac wall. Our data indicate p1159 decreases LOX2 expression in a sex-specific manner. Reduced collagen cross-linking in females would mean increased LV compliance and contractility, which could also explain the improved EF observed in females.

3.4. p1159 increases vessel perfusion in the infarct LV

To investigate whether p1159 has pro-angiogenic effects in vivo, we systemically injected GS-IB_4 2 h prior to euthanasia of mice treated ± p1159 for 14 days post-MI. Isolectin binds to sugar residues of blood vessels showing vessel perfusion and it also identifies the formation of neovascular structures from the endocardium [32,33]. We counterstained the samples with an anti-CD31 (platelet endothelial cell adhesion molecule 1) antibody, a potent marker for endothelial cell-cell junction [34], to scale for total vessels. Both markers were imaged (Fig. 3A) and quantified by the percentage area of IF staining on the LV remote and infarct zones. In the remote zone, total vessels area was decreased in p1159-treated mice, compared to vehicle control; however, no changes were observed in the infarct zone between treatments (Fig. 3B). On the other hand, while perfused vessel area was similar between groups in the remote area, peptide-treated animals presented a significant increase of GS-IB_4^+ in the infarct zone compared to controls (Fig. 3C), suggesting p1159 promoted vessel perfusion in the injured tissue. To confirm this result, we calculated the ratio of perfused/total vessel area (Fig. 3D). Animals that received p1159 therapy had increased area of functional/perfused vessels in the infarcted area, indicating that p1159 supports vessel perfusion during the repair of the damaged heart.

3.5. p1159 binds to integrin alpha 4 to stimulate cardiac fibroblast migration

The process of cardiac repair in the infarcted site is highly regulated by inflammatory and interstitial cells; of the latter, fibroblasts are the key mediators responsible for secreting the fibrogenic components to form the scar post-MI that will replace the necrotic loss of cardiomyocytes [35]. To investigate the direct effects of p1159 in fibroblasts, we isolated LV fibroblasts from naïve mice and stimulated cells with different doses of the peptide (100 nM and 500 nM). The peptide did not induce cell proliferation, differentiation, or cytotoxicity (data not shown). Using an automated wound healing assay, we observed a marked increase in migration rates compared to the negative control; noteworthy, the 100 nM dose diluted in serum free media presented similar migratory effects to those of the positive control group (complete media, Fig. 4A). These data suggest that p1159 acts either as a direct ligand for fibroblasts to induce cell motility or indirectly by affecting cell substrate surface to promote migration; in vivo, this could impact myocardial healing since enhanced cell migration affects LV remodeling

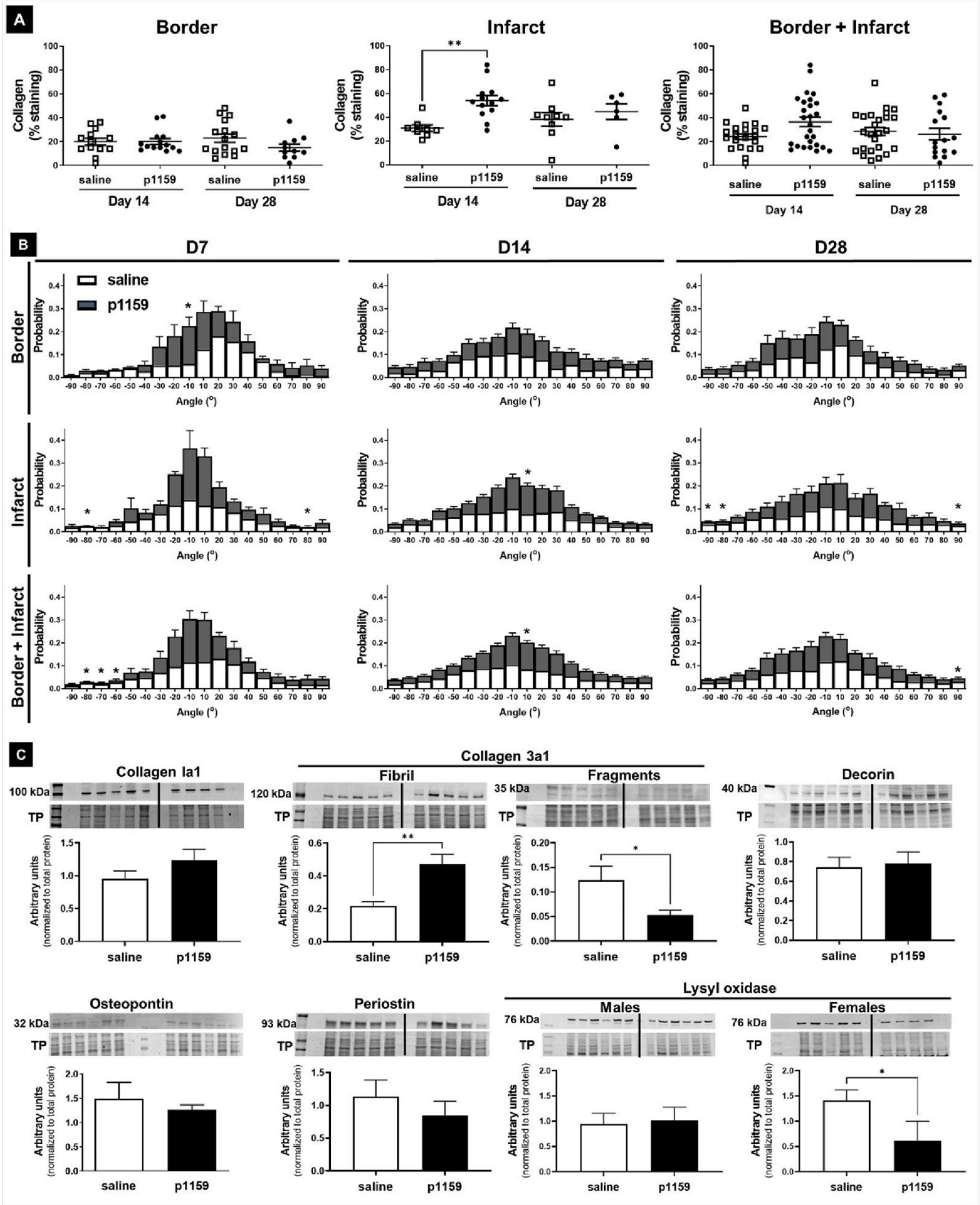

(caption on next page)

Fig. 2. Long term treatment with p1159 alters scar composition and fiber alignment. A. Total collagen content. The border zone did not show any differences in total collagen staining. However, at D14 p1159 presented increased levels of collagen compared to control. Combined quantification (infarct and border) did not show groups differences. n = 21–24/group. B. Profile of collagen fibers alignment in relation to the pericardium. Collagen fiber alignment, represented in stacked bar graphs, was significantly different between treatments. Specifically, at D7 and D14 the peptide-treated groups displayed more fibers aligned at −10/10° respectively in the border and infarct zones. Conversely, the vehicle group displayed more misaligned fibers (−80/80°) at these time points. At D28, vehicle and peptide groups displayed comparable levels of circumferentially aligned fibers (−10 to 10°); however, the vehicle groups showed higher amounts of misaligned fibers at −90, −80, and 80°. *p < 0.05 versus same fiber angle saline. C. Scar composition at D28. Extracellular matrix proteins were quantified by immunoblotting in LVI lysates. No changes were observed with peptide treatment in collagen 1, decorin, osteopontin, and periostin. Nonetheless, p1159 promoted secretion of collagen type 3. Of note, collagen type 3 fragmentation was reduced in p1159 LVIs. Although combined data did not display statistical differences between groups, p1159-treated females showed reduced scar cross-linking as measured by lysyl oxidase content. Data are normalized to total protein (TP, loading control) and presented as average ± SEM, n = 5–6/group.

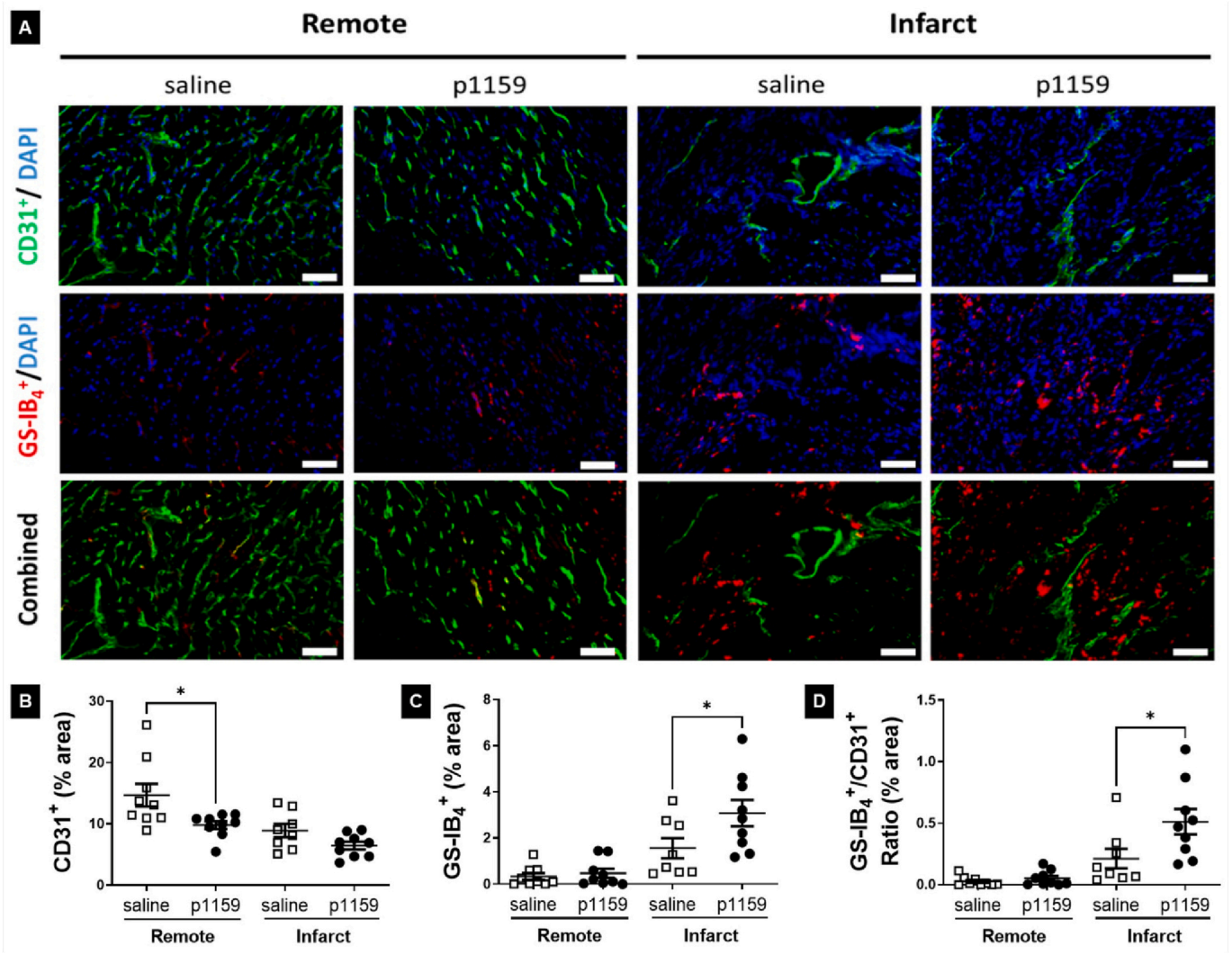

Fig. 3. Long term treatment with p1159 alters vessel perfusion post-MI. A. Representative images of LV tissue stained for total vessel numbers (green, CD31+), perfused vessels (red, isolectin+), and nuclei (blue, DAPI) in the remote (left panels) and infarcted (right panels) areas. B. Total vessel numbers. While less vessels were observed in p1159 treated animals in the remote region, no difference was present between groups in the infarcted area. C. Perfused vasculature. p1159 treatment increased vessel perfusion in the infarcted area. D. Perfused/total vessels ratio. p1159 treated mice displayed increased ratio of perfused vessels per total vessel numbers in the infarcted zone. *$p < 0.05$ between groups. (For interpretation of the references to color in this figure legend, the reader is referred to the web version of this article.)

during the reparative phase post-MI [36]. Fibroblast migration occurs by adhesive interactions between cell surface proteins, specially integrins, and the surrounding ECM [37]. From the reported matricryptins, several cellular receptors have already been identified and integrins represent most of the receptors for matricryptic sites (~41 %) [11]. To evaluate changes in receptor expression involved in p1159-mediated fibroblast migration, we used D7 tissues from our MI tissue bank (± p1159 treatment) to run a gene array panel for ECM molecules and receptors that included 13 integrins. Overexpression of integrin alpha 3 (Itgα3), Itgα4, Itgαm, Itgβ1, Itgβ2, and Itgβ3 were found in the infarcted area of p1159 treated mice (supplemental Fig. S3); of these, Itgα4 presented a 3-fold increase compared to control (Fig. 4B, mRNA and protein).

To validate these findings, we used the same automated wound healing assay with LV fibroblasts. At time of confluence, cells were incubated ± blocking antibody (Ab) against Itgα4 diluted in SFM for 2 h prior to wounding. After wounding, media was replaced with SFM ±

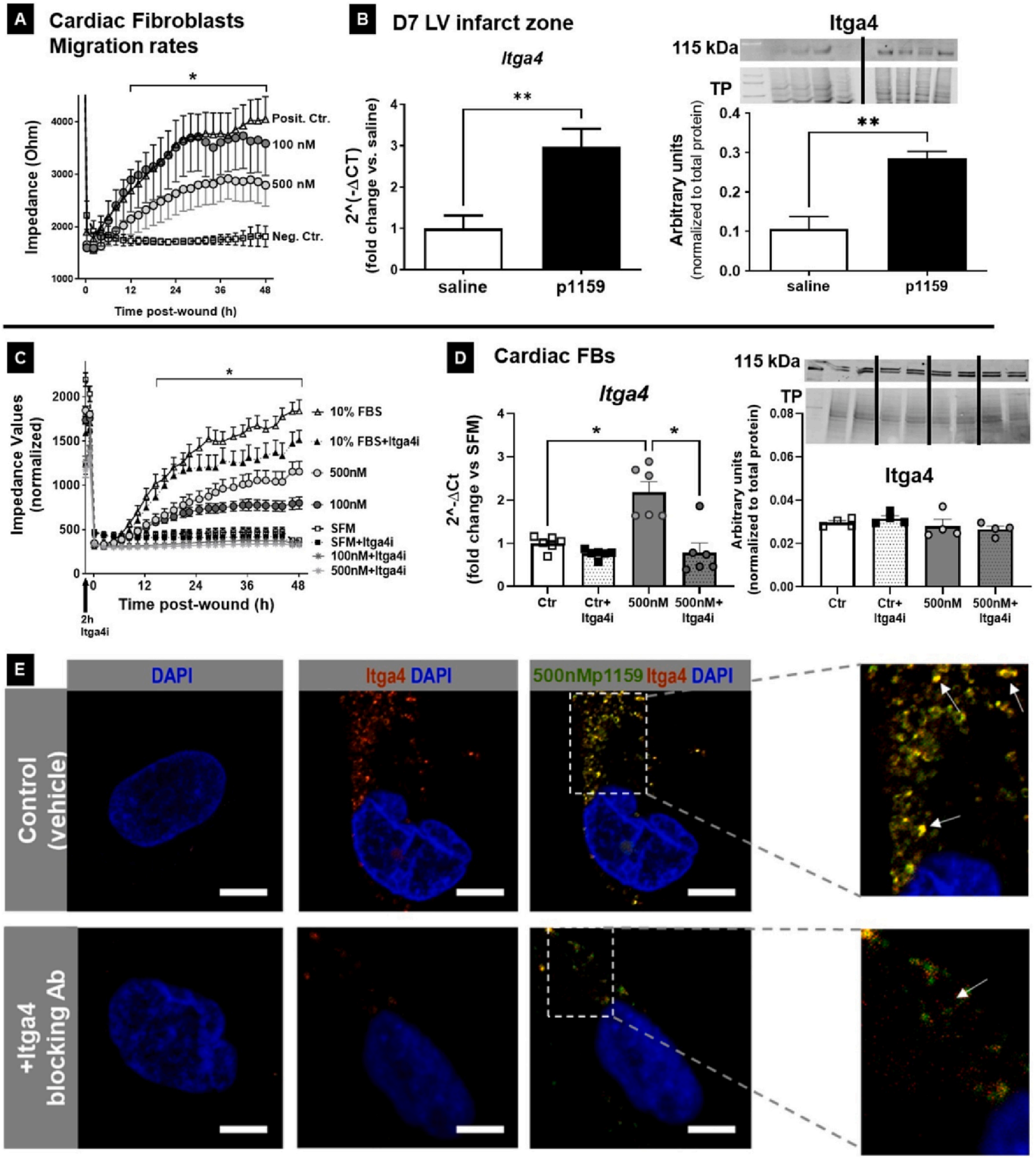

Fig. 4. p1159 promotes fibroblast migration and this may occur via integrin-α4 (Itgα4). A. LV fibroblasts treated with p1159 (100 nM in serum free media, SFM) presented a significant increase in migration rate, which was similar to the positive control (10 % FBS), demonstrating strong pro-migratory properties. *$p < 0.05$ p1159 100 nM and 500 nM versus negative control (SFM); $n = 6$/group. B. p1159 in vivo treatment induces overexpression of Itgα4 post-MI. Left panel: mRNA levels n = 6/group; right panel: representative immunoblot image, TP = total protein stain (loading control), $n = 4$/group. **$p < 0.01$. C. The neutralizing antibody against Itga4 inhibited p1159 induced fibroblast migration. Positive control (10 % FBS), negative control (SFM), and p1159 (100 nM and 500 nM) were treated ± Itgα4 neutralizing antibody (Itga4i). The impedance values were normalized before incubation with Itga4i and after wound. *$p < 0.05$ represents when both concentrations of p1159 statistically differed from its respective groups with Itga4i, and from the negative controls; n = 6/group. D. Cardiac fibroblasts stimulated with p1159 overexpress Itga4 mRNA and this effect is abolished in the presence of Itga4i. Left panel: mRNA levels n = 6/group; right panel: representative immunoblot image, TP = total protein stain (loading control), n = 4/group. *p < 0.05 E. Itgα4 (red) co-localized with p1159 (green, FITC labeled) in human cardiac fibroblasts (HCF) and that effect was inhibited in the presence of Itga4i. Blue = nuclei, yellow = co-localization. Scale bar = 5 μm. All graphs display average ± SEM. (For interpretation of the references to color in this figure legend, the reader is referred to the web version of this article.)

p1159 or positive control (complete media). The blocking antibody completely abolished the peptide-induced cell migration, suggesting Itgα4 is a fibroblast receptor for the collagen-derived peptide p1159 (Fig. 4C). We also tested the positive and negative controls ± Itgα4 blocking Ab and we did not see changes in the migratory profiles, giving evidence that the blocking antibody on its own does not inhibit migration. Itgα4 is known to bind to fibronectin, thrombospondin, and VCAM-1 but it has not been reported to bind to collagen [38,39]. Our in vivo data showed that Itgα4 is highly expressed in the infarcted LV of p1159-treated mice at 7 days post-MI, with a 3-fold increase compared to vehicle controls (Fig. 4B, mRNA and protein) and this was confirmed in fibroblasts mRNA in vitro (Fig. 4D). Protein levels of Itga4 did not differ between groups in cultured fibroblasts under the conditions tested. These experiments were validated in primary mouse LV fibroblasts and in human cardiac fibroblasts (HCF). While primary mouse fibroblasts were used at P2 and HCF at P5, we cultured all cells on gelatin coated flasks to prevent cell differentiation. However, it is possible that at P5 HCF could have some degree of fibroblast differentiation into myofibroblasts. If that was the case, we would expect to see increased levels of Itgα4 in HCF, since Itgα4 has been reported to be overexpressed in myofibroblasts compared to quiescent fibroblasts [40]. Finally, using a FITC-labeled peptide we confirmed in vitro co-localization of p1159 and Itgα4 (Fig. 4E).

3.6. p1159 activates Rho pathways in fibroblasts

Several pathways have been reported to be involved in cell adhesion and migration [41–43]. We used a motility gene array to investigate the signaling pathways involved in p1159-induced fibroblast migration by the Itgα4 receptor. We found Rho GDP-dissociation inhibitor 1 alpha (RhoGDIα), a molecule from the Rho GTPase pathway, to be changed upon p1159 treatment. RhoGDI is a cytosolic molecule that holds inactive Rho (GDP) preventing the continuation of the active (GTP-bound) and inactive (GDP-bound) cycle in the membrane [44]. RhoGDI was decreased by peptide treatment and the effect was abolished with the use of Itgα4 blocking Ab (Fig. 5A). To further test whether Rho GTPases are involved in p1159-induced fibroblast migration via Itgα4, we incubated fibroblasts (~50 % confluence) with Itgα4 blocking Ab for 2 h in SFM followed by addition of p1159 (100 nM or 500 nM) or respective controls (see Table 1); media was removed, and cells fixed at different timepoints (3, 5 and 15 min post-p1159 treatment). Immunofluorescent (IF) revealed that, like the positive control, Itgα4 and RhoA signals are highly increased in fibroblasts after 15 min treatment with p1159, at both 100 nM and 500 nM doses (Fig. 5B, left panels). Notably, cells that were previously incubated with Itgα4 blocking Ab presented very weak IF signals of Itgα4 and RhoA activation, which was similar to the negative control (Fig. 5B, right panels). The 3- and 5-minute treatments did not show differences compared to the controls (data not shown). Further investigations are required for a better understanding of how RhoA is activated in fibroblasts when the upstream signal is triggered by p1159.

4. Discussion

Our previous in vivo study, which evaluated cardiac changes post-MI during p1159 short-term treatment (7 days), demonstrated that male mice treated with p1159 display reduced LV dilation and fibrosis compared to controls [14]. An important goal of this study was to extend our previous findings to evaluate whether, and how, long-term peptide treatment prevents adverse cardiac remodeling post-MI. We also expanded our design to include both sexes to verify if p1159 acts in a sex-specific manner. Compared to controls, animals treated with p1159 displayed a robust increase in EF signing an improvement in systolic function. Additionally, p1159 significantly reduced LV dilation (lower LV internal diameter and volume both at systole and diastole). Even though the EF in peptide-treated mice is <40 % (threshold generally accepted for systolic dysfunction in humans) at D28, it is important to note that we used a model of permanent occlusion and these animals did not received reperfusion. Therefore, a 2-fold increase in EF in a non-reperfused infarcted LV is physiologically significant. Together, these results indicate that p1159 long-term therapy attenuates eccentric remodeling post-MI, which results in decreased chamber volumes and

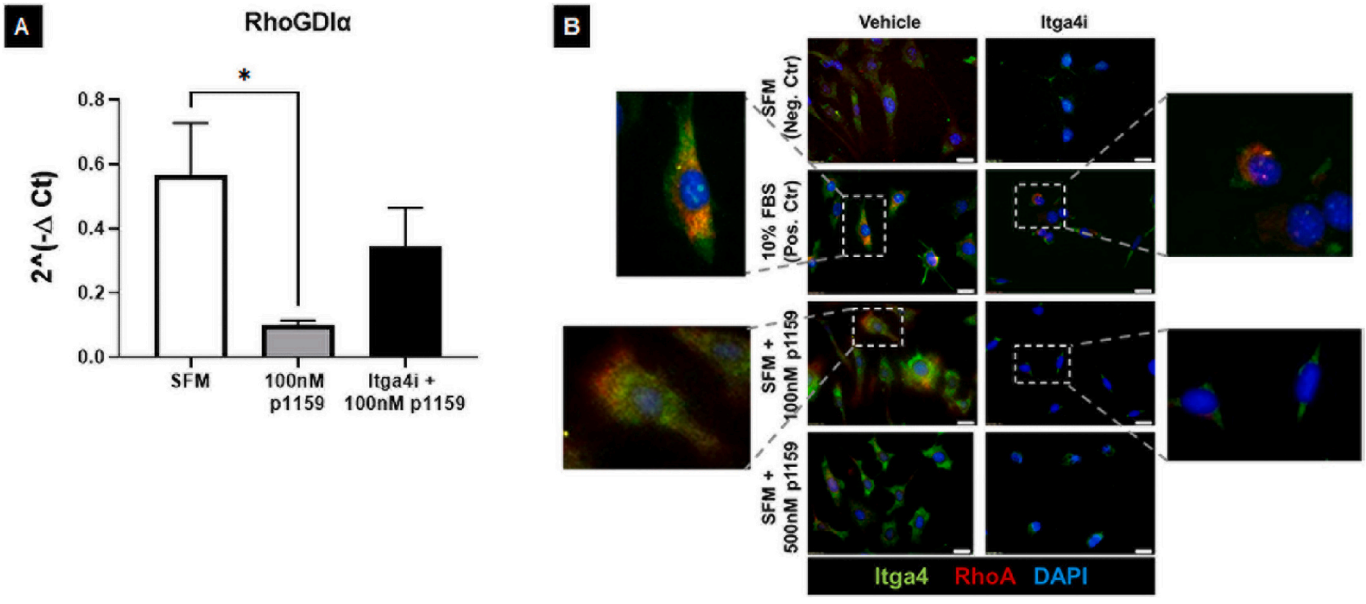

Fig. 5. p1159-induced migration may occur via Rho GTPase pathways. A. p1159-treatment reduced RhoGDI expression, and this effect was dependent on Itgα4. Gene expression of cardiac fibroblasts treated with p1159 100 nM ± Itgα4 blocking antibody (Ab) and negative control (SFM). *$p < 0.05$ versus negative control (SFM), $^{\#}p < 0.05$ versus 100 nM p1158/59. B. p1159 induces RhoA activation in fibroblasts. Representative immunofluorescence images of fibroblasts treated with negative control (SFM), positive control (10 % FBS) and SFM ± p1159 100 nM or 500 nM, indicating stimulation of Itgα4 receptor (green) and activation of RhoA (red). Right panels: Representative images of the same groups incubated 2 h prior with blocking antibody against Itgα4 (Itga4 Ab), indicating that both Itgα4 receptor and RhoA signals were strongly decreased by fibroblasts treated with p1159 in the presence of the Ab. Magnification/scale bars: 20× = 50 μm; 40× = 20 μm. (For interpretation of the references to color in this figure legend, the reader is referred to the web version of this article.)

LV internal dimensions.

Alterations in the cardiac function post-MI are caused not only by changes in the shape and size of the LV and the scar, but also by the molecular structure and intrinsic composition of the fibrotic scar and cardiac tissue. While an excessive fibrotic response is harmful and can cause progressive cardiac dysfunction, the first reparative fibrosis is essential for preventing ventricular wall rupture [45]. In our study, the vehicle control group had a 32 % mortality rate (10/31 mice died) and the p1159 group had 17 % mortality (5/29 animals); of these 60 % displayed LV rupture (6/10 saline and 3/5 peptide). Due to the disparity in mortality rates, we were not able to determine peptide effects on LV rupture. Next, we measured the overall levels of interstitial fibrosis in the infarcted scar. Since we observed such a striking difference between treatments in LV dilation and function, we were surprised to note that by D28 both groups had similar levels of interstitial fibrosis.

Further investigation led us to look at the structure and composition of the scar. Myofiber orientation in the infarcted scar is an important variable that defines the compliance and biomechanical properties of the LV post-MI [46,47]. Throughout the study, the infarct zone of p1159-treated mice presented increased numbers of fibers with angles close to 0° (parallel to the epicardium). In contrast, at the end of the study (D28) the control group showed significantly increased number of fibers perpendicular to the pericardium. These findings indicate that collagen fibers are more organized in the infarcted scar of the peptide group during the healing process. Studies have shown that LV scars containing a large percentage of collagen fibers oriented parallel to the circumferential section (i.e. pericardium) tend to resist excessive circumferential stretching, and usually deform in the radial and longitudinal directions similarly to the noninfarcted myocardium [48]. Dr. Holmes group developed a finite-element model of a LV infarct to explore a wide range of infarct mechanical properties, including fiber alignment [49]. They identified that the infarct zone with high longitudinal stiffness, but low circumferential stiffness, can increase EDV, leading to the best stroke volume [49]. In addition, Costa et al. demonstrated that an heterogenous fiber orientation, compared to a homogeneous pattern, can result in more reduced anisotropy and higher local stress levels leading to impaired cardiac function that may lead to LV rupture [50]. The parallel alignment of collagen fibers is an indicative that the scar is less stiff and more compliant, while being resistant to excessive stretching. Our data suggest p1159 treatment promotes fiber alignment parallel to the epicardium, which leads to low circumferential stiffness, promotes tissue compliance, and favors the formation of more functional scar. This result could explain how p1159 treatment preserves LV integrity by reducing chamber dilation and improving systolic function. The formation of new collagen fibers and their alignment will constitute the restored myocardium and dictate the biomechanical properties and elasticity of the scar post-MI [51]. We then determined which type of collagen fibers were present in the infarcted scar. While fibrillar collagen type I is organized in parallel to other fibrils and it is highly resistant to compliance, fibrillar collagen type III is the first collagen to be secreted after a wound and it is more compliant than collagen type I [52]. Though no differences were detected in levels of collagen type I, collagen type III was increased in the p1159 group. An increase in collagen III levels leads to a more compliant, less stiff, scar that can more easily expand with blood inflow followed by favoring the blood outflow with the contraction. This is in accordance with the functional data, as peptide-treated mice presented improved ejection fraction, compared to controls, demonstrating that p1159 treatment conferred increased scar compliance. Moreover, increased compliance can also contribute to adaptive remodeling by decreasing LV dilation, which was also observed upon p1159 treatment (decreased EDV and ESV compared to controls). Finally, this decrease in LV eccentric remodeling is also validated by the decrease in LV internal diameter during systole and diastole (LVIDs and LVIDd). In accordance with this notion, LOX2 levels were reduced, compared to controls, in females treated with p1159, indicating decreased fiber cross-linking and therefore a more compliant scar. Fiber deposition, cross-linking, maturation, and degradation are all part of ECM dynamic remodeling after the LV injury. LOX plays a critical role by regulating cross-linking between ECM fibers. However, high levels of LOX may promote early cross-linking, which can be detrimental: first, by not allowing enough time for an appropriate arrangement of ECM fibers causing impaired fibrosis; and second, continuous cross-linking can increase the stiffness of the scar leading to decreased compliance. Together, our proteomics data indicate p1159 increases LV compliance which favors an increase in ejection fraction. These data help to explain the observed improved cardiac function. Our data support the notion that p1159 attenuates adverse remodeling through generation of a more compliant tissue by promoting collagen type III presence, improving fiber alignment, and reducing cross-linking in the infarcted scar, more specifically in females.

To further investigate mechanisms that could explain improved systolic function with peptide-treatment we measured vessel numbers and perfusion in the infarcted LV. After an ischemic event, fibroblasts and endothelial cells (ECs) undergo proliferation to form a vascularized granulation tissue that will mature into the fibrotic-rich scar [53,54]. Angiogenesis is essential for tissue healing and regeneration post-injury and, in mice, the angiogenic process occurs between days 7–21 post-MI [55]. ECM and matricryptic sites participate in the regulation of angiogenesis during remodeling and tissue healing [11]. Several studies describe specific matricryptins as potent anti- or pro-angiogenic factors [56,57]. Our previous study showed that p1159 may interact with human umbilical vascular endothelial cells to induce the formation of vasculogenic networks in vitro [14]. p1159 treated LVs displayed increased area of functional/perfused vessels in the infarcted area, suggesting p1159 supports vessel perfusion. Although these data are preliminary and further studies need to look at the underlying mechanisms, these results suggest that p1159 may accelerate tissue healing in the ischemic zone. The restoration of blood flow surrounding the ischemic injury prevents loss of cardiomyocytes and maintains local homeostasis [53]. Thus, the formation of new vessels in the border zone is critical during cardiac remodeling. Interestingly, both total and perfused vessel numbers were similar in the border zone of vehicle control and p1159-treated mice at D14 (data not displayed). Together, these results suggest p1159 is not pro-angiogenic, since we did not observe increased total vessels area, but supports vessel perfusion. Further studies will focus on the mechanisms underlying increased vessel perfusion in the infarcted area resulting from p1159 therapy.

Finally, our in vitro studies demonstrate p1159 markedly increases cardiac fibroblast migration and this effect is mediated by the membrane receptor Itgα4. Integrins are transmembrane receptors that mediate the interactions between ECM and the actin cytoskeleton during cell adhesion and migration [37]. A motility gene array revealed p1159 decreased expression of RhoGDI, a component from the Rho GTPase pathway. Importantly, the effect was abolished with the use of an Itgα4 blocking antibody. Typically, Rho family GTPases act as molecular switches cycling between inactive and active forms [58]. RhoGDI functions by extracting Rho family GTPases from membranes and solubilizing them in the cytosol; therefore, reduced RhoGDI suggests higher levels of membrane-bound GTPases, which would lead to increased migration. These results both support Itgα4 as one receptor for p1159 in fibroblasts and demonstrate that RhoA plays a key role in the peptide induced fibroblast migration.

In summary, our study showed that compared to vehicle control, p1159 treatment significantly increased fibroblast migration, promoted deposition of collagen III in the post-MI scar, led to collagen fiber alignment parallelly to the epicardium, and resulted in increased vessel perfusion. These mechanisms likely work in concert to improve EF. An increase in fibroblast migration may result in an earlier deposition of scar components, which allows for more time for appropriate fiber alignment. This in turn could result in lower circumferential stiffness and a more homogeneous fiber orientation that increases tissue compliance. Similarly, higher levels of collagen III also enhance tissue

compliance. Together, the reduction in myocardial stiffness and increase in myocardial compliance explain the improved EF. Finally, the observed higher number of perfused vessels in the infarcted area of p1159 animals, suggests a more functional myocardial scar, which would also favor improved systolic function.

5. Conclusions

This study identified Itgα4 as a potential receptor for matricryptin p1159; additionally, we showed p1159 may regulate different cell types, i.e. cardiac fibroblasts and ECs, and modulates tissue composition during cardiac remodeling post-MI. Our data show that matricryptin p1159 attenuates adverse remodeling by stimulating cardiac fibroblast migration, via Itgα4 receptor, to promote an earlier and organized maturation of the infarct scar, thus decreasing LV dilation. Noteworthy, p1159 treatment promoted vessel perfusion in the ischemic injury, to preserve local homeostasis and structural integrity, and improved systolic function in a non-reperfused MI model. The present study is the first study to show that bioactive small extracellular matrix peptides (i.e. matricryptins) could be candidate therapeutic targets for pathologies where a vascular and stable scar are necessary. Additional research is needed to investigate the use of matricryptins that may be potentially useful for the treatment of human cardiac injury and remodeling.

Funding disclosures

This work was supported by East Carolina University, the American Heart Association [grant numbers 18AIREA33960311 and 19PRE34450066], and the National Institutes of Health - National Heart, Lung, and Blood Institute [grant number HL152297]. The authors have no competing interests to declare.

Data availability

The authors declare that all supporting data are available within the article and its Data Supplement. Expanded methods sections for the in vitro assays, surgery, RNA and protein extraction, immunobloting, RT-PCR expression analysis, immunohistochemistry, immunofluorescence, and ultrasound image analysis are available in the Data Supplement. Representative images were selected to represent quantification results shown with the images. Assay procedures and quantification analysis for in vivo experiments were performed by scientists (P.R.S. and S.N.C), who were not aware of treatment group.

Acknowledgements

We acknowledge the technical contribution of Hamilton J. Stoffel, B. Sc.; Caleb Anthony Morrow, B.Sc.; Octavious T. Johnson, M.Sc.; and Emma J. Goldberg, B.Sc.

Appendix A. Supplementary data

Supplementary data to this article can be found online at https://doi.org/10.1016/j.lfs.2023.121598.

References

[1] C.W. Tsao, A.W. Aday, Z.I. Almarzooq, A. Alonso, A.Z. Beaton, M.S. Bittencourt, A. K. Boehme, A.E. Buxton, A.P. Carson, Y. Commodore-Mensah, M.S.V. Elkind, K. R. Evenson, C. Eze-Nliam, J.F. Ferguson, G. Generoso, J.E. Ho, R. Kalani, S.S. Khan, B.M. Kissela, K.L. Knutson, D.A. Levine, T.T. Lewis, J. Liu, M.S. Loop, J. Ma, M. E. Mussolino, S.D. Navaneethan, A.M. Perak, R. Poudel, M. Rezk-Hanna, G.A. Roth, E.B. Schroeder, S.H. Shah, E.L. Thacker, L.B. VanWagner, S.S. Virani, J.H. Voecks, N.-Y. Wang, K. Yaffe, S.S. Martin, Heart disease and stroke statistics—2022 update: a report from the American Heart Association, Circulation 145 (8) (2022) e153–e639.

[2] Y. Gerber, S.A. Weston, M.M. Redfield, A.M. Chamberlain, S.M. Manemann, R. Jiang, J.M. Killian, V.L. Roger, A contemporary appraisal of the heart failure epidemic in Olmsted County, Minnesota, 2000 to 2010, JAMA Intern. Med. 175 (6) (2015) 996–1004.

[3] E.J. Benjamin, P. Muntner, A. Alonso, M.S. Bittencourt, C.W. Callaway, A. P. Carson, A.M. Chamberlain, A.R. Chang, S. Cheng, S.R. Das, F.N. Delling, L. Djousse, M.S.V. Elkind, J.F. Ferguson, M. Fornage, L.C. Jordan, S.S. Khan, B. M. Kissela, K.L. Knutson, T.W. Kwan, D.T. Lackland, T.T. Lewis, J.H. Lichtman, C. T. Longenecker, M.S. Loop, P.L. Lutsey, S.S. Martin, K. Matsushita, A.E. Moran, M. E. Mussolino, M. O'Flaherty, A. Pandey, A.M. Perak, W.D. Rosamond, G.A. Roth, U. K.A. Sampson, G.M. Satou, E.B. Schroeder, S.H. Shah, N.L. Spartano, A. Stokes, D. L. Tirschwell, C.W. Tsao, M.P. Turakhia, L.B. VanWagner, J.T. Wilkins, S.S. Wong, S.S. Virani, Heart disease and stroke statistics-2019 update: a report from the American Heart Association, Circulation 139 (10) (2019) e56–e528.

[4] P.L. Laforgia, C. Auguadro, S. Bronzato, A. Durante, The reduction of mortality in acute myocardial infarction: from bed rest to future directions, Int. J. Prev. Med. 13 (2022) 56.

[5] L. Khalid, S.H. Dhakam, A review of cardiogenic shock in acute myocardial infarction, Curr. Cardiol. Rev. 4 (1) (2008) 34–40.

[6] M. Afana, W. Brinjikji, H. Cloft, S. Salka, Hospitalization costs for acute myocardial infarction patients treated with percutaneous coronary intervention in the United States are substantially higher than Medicare payments, Clin. Cardiol. 38 (1) (2015) 13–19.

[7] M.P. Czubryt, Common threads in cardiac fibrosis, infarct scar formation, and wound healing, Fibrogenesis Tissue Repair 5 (1) (2012) 19.

[8] N. Frey, H.A. Katus, E.N. Olson, J.A. Hill, Hypertrophy of the heart: a new therapeutic target? Circulation 109 (13) (2004) 1580–1589.

[9] G.E. Davis, K.J. Bayless, M.J. Davis, G.A. Meininger, Regulation of tissue injury responses by the exposure of matricryptic sites within extracellular matrix molecules, Am. J. Pathol. 156 (5) (2000) 1489–1498.

[10] M. Donet, S. Brassart-Pasco, S. Salesse, F.X. Maquart, B. Brassart, Elastin peptides regulate HT-1080 fibrosarcoma cell migration and invasion through an Hsp90-dependent mechanism, Br. J. Cancer 111 (1) (2014) 139–148.

[11] S. Ricard-Blum, S.D. Vallet, Matricryptins network with matricellular receptors at the surface of endothelial and tumor cells, Front. Pharmacol. 7 (2016) 11.

[12] N. Liu, R.K. Lapcevich, C.B. Underhill, Z. Han, F. Gao, G. Swartz, S.M. Plum, L. Zhang, S.J. Green, Metastatin: a hyaluronan-binding complex from cartilage that inhibits tumor growth, Cancer Res. 61 (3) (2001) 1022–1028.

[13] G. Liu, M.A. Cooley, A.G. Jarnicki, T. Borghuis, P.M. Nair, G. Tjin, A.C. Hsu, T. J. Haw, M. Fricker, C.L. Harrison, B. Jones, N.G. Hansbro, P.A. Wark, J.C. Horvat, W.S. Argraves, B.G. Oliver, D.A. Knight, J.K. Burgess, P.M. Hansbro, Fibulin-1c regulates transforming growth factor–β activation in pulmonary tissue fibrosis, JCI Insight 4 (16) (2019), e124529.

[14] M.L. Lindsey, R.P. Iyer, R. Zamilpa, A. Yabluchanskiy, K.Y. DeLeon-Pennell, M. E. Hall, A. Kaplan, F.A. Zouein, D. Bratton, E.R. Flynn, P.L. Cannon, Y. Tian, Y. F. Jin, R.A. Lange, D. Tokmina-Roszyk, G.B. Fields, L.E. de Castro Bras, A. Novel, Collagen matricryptin reduces left ventricular dilation post-myocardial infarction by promoting scar formation and angiogenesis, J. Am. Coll. Cardiol. 66 (12) (2015) 1364–1374.

[15] M.L. Lindsey, K.R. Brunt, J.A. Kirk, P. Kleinbongard, J.W. Calvert, L.E. de Castro Brás, K.Y. DeLeon-Pennell, D.P. Del Re, N.G. Frangogiannis, S. Frantz, R.J. Gumina, G.V. Halade, S.P. Jones, R.H. Ritchie, F.G. Spinale, E.B. Thorp, C.M. Ripplinger, Z. Kassiri, Guidelines for in vivo mouse models of myocardial infarction, Am. J. Physiol. Heart Circ. Physiol. 321 (6) (2021) H1056–h1073.

[16] Guide for the Care and Use of Laboratory Animals, The National Academies Collection, National Academies Press (US), Washington (DC), 2011.

[17] L.J. Feldman, D. Himbert, J.M. Juliard, G.J. Karrillon, H. Benamer, P. Aubry, O. Boudvillain, P. Seknadji, M. Faraggi, G. Steg, Reperfusion syndrome: relationship of coronary blood flow reserve to left ventricular function and infarct size, J. Am. Coll. Cardiol. 35 (5) (2000) 1162–1169.

[18] F. Thuny, O. Lairez, F. Roubille, N. Mewton, G. Rioufol, C. Sportouch, I. Sanchez, C. Bergerot, H. Thibault, T.T. Cung, G. Finet, L. Argaud, D. Revel, G. Derumeaux, E. Bonnefoy-Cudraz, M. Elbaz, C. Piot, M. Ovize, P. Croisille, Post-conditioning reduces infarct size and edema in patients with ST-segment elevation myocardial infarction, J. Am. Coll. Cardiol. 59 (24) (2012) 2175–2181.

[19] G.M. Fomovsky, J.W. Holmes, Evolution of scar structure, mechanics, and ventricular function after myocardial infarction in the rat, Am. J. Physiol. Heart Circ. Physiol. 298 (1) (2010) H221–H228.

[20] W.J. Karlon, J.W. Covell, A.D. McCulloch, J.J. Hunter, J.H. Omens, Automated measurement of myofiber disarray in transgenic mice with ventricular expression of ras, Anat. Rec. 252 (4) (1998) 612–625.

[21] M.L. Lindsey, G.A. Gray, S.K. Wood, D. Curran-Everett, Statistical considerations in reporting cardiovascular research, Am. J. Physiol. Heart Circ. Physiol. 315 (2) (2018) H303–H313.

[22] B.A. French, C.M. Kramer, Mechanisms of post-infarct left ventricular remodeling, Drug Discov. Today Dis. Mech. 4 (3) (2007) 185–196.

[23] C.S.P. Lam, M. McEntegart, B. Claggett, J. Liu, H. Skali, E. Lewis, L. Køber, J. Rouleau, E. Velazquez, R. Califf, J.J. McMurray, M. Pfeffer, S. Solomon, Sex differences in clinical characteristics and outcomes after myocardial infarction: insights from the valsartan in acute myocardial infarction trial (VALIANT), Eur. J. Heart Fail. 17 (3) (2015) 301–312.

[24] A. Aimo, G. Panichella, A. Barison, S. Maffei, M. Cameli, S. Coiro, F. D'Ascenzi, C. Di Mario, R. Liga, R. Marcucci, D. Morrone, I. Olivotto, I. Tritto, M. Emdin, Sex-related differences in ventricular remodeling after myocardial infarction, Int. J. Cardiol. 339 (2021) 62–69.

[25] R. Zamilpa, J. Zhang, Y.A. Chiao, L.E. de Castro Brás, G.V. Halade, Y. Ma, S. O. Hacker, M.L. Lindsey, Cardiac wound healing post-myocardial infarction: a

novel method to target extracellular matrix remodeling in the left ventricle, Methods Mol. Biol. (2013, 1037) 313–324.
[26] C.Y. Ewald, The matrisome during aging and longevity: a systems-level approach toward defining matreotypes promoting healthy aging, Gerontology 66 (3) (2019) 266–274.
[27] I. Abdelaziz Mohamed, A.P. Gadeau, A. Hasan, N. Abdulrahman, F. Mraiche, Osteopontin: a promising therapeutic target in cardiac fibrosis, Cells 8 (12) (2019) 1558–1572.
[28] S.M. Weis, S.D. Zimmerman, M. Shah, J.W. Covell, J.H. Omens, J. Ross Jr., N. Dalton, Y. Jones, C.C. Reed, R.V. Iozzo, A.D. McCulloch, A role for decorin in the remodeling of myocardial infarction, Matrix Biol. 24 (4) (2005) 313–324.
[29] M. Shimazaki, K. Nakamura, I. Kii, T. Kashima, N. Amizuka, M. Li, M. Saito, K. Fukuda, T. Nishiyama, S. Kitajima, Y. Saga, M. Fukayama, M. Sata, A. Kudo, Periostin is essential for cardiac healing after acute myocardial infarction, J. Exp. Med. 205 (2) (2008) 295–303.
[30] Z. Chen, J. Xie, H. Hao, H. Lin, L. Wang, Y. Zhang, L. Chen, S. Cao, X. Huang, W. Liao, J. Bin, Y. Liao, Ablation of periostin inhibits post-infarction myocardial regeneration in neonatal mice mediated by the phosphatidylinositol 3 kinase/glycogen synthase kinase 3β/cyclin D1 signalling pathway, Cardiovasc. Res. 113 (6) (2017) 620–632.
[31] J. González-Santamaría, M. Villalba, O. Busnadiego, M.M. López-Olañeta, P. Sandoval, J. Snabel, M. López-Cabrera, J.T. Erler, R. Hanemaaijer, E. Lara-Pezzi, F. Rodríguez-Pascual, Matrix cross-linking lysyl oxidases are induced in response to myocardial infarction and promote cardiac dysfunction, Cardiovasc. Res. 109 (1) (2016) 67–78.
[32] K. Kobayashi, K. Maeda, M. Takefuji, R. Kikuchi, Y. Morishita, M. Hirashima, T. Murohara, Dynamics of angiogenesis in ischemic areas of the infarcted heart, Sci. Rep. 7 (1) (2017) 7156.
[33] R.L. Benton, M.A. Maddie, D.R. Minnillo, T. Hagg, S.R. Whittemore, Griffonia simplicifolia isolectin B4 identifies a specific subpopulation of angiogenic blood vessels following contusive spinal cord injury in the adult mouse, J. Comp. Neurol. 507 (1) (2008) 1031–1052.
[34] P. Lertkiatmongkol, D. Liao, H. Mei, Y. Hu, P.J. Newman, Endothelial functions of platelet/endothelial cell adhesion molecule-1 (CD31), Curr. Opin. Hematol. 23 (3) (2016) 253–259.
[35] Y. Sun, Myocardial repair/remodelling following infarction: roles of local factors, Cardiovasc. Res. 81 (3) (2009) 482–490.
[36] C. Humeres, N.G. Frangogiannis, Fibroblasts in the infarcted, remodeling, and failing heart, JACC Basic Transl.Sci. 4 (3) (2019) 449–467.
[37] A. Huttenlocher, A.R. Horwitz, Integrins in cell migration, Cold Spring Harb. Perspect. Biol. 3 (9) (2011), a005074.
[38] M.J. Calzada, L. Zhou, J.M. Sipes, J. Zhang, H.C. Krutzsch, M.L. Iruela-Arispe, D. S. Annis, D.F. Mosher, D.D. Roberts, α4β1 integrin mediates selective endothelial cell responses to thrombospondins 1 and 2 in vitro and modulates angiogenesis in vivo, Circ. Res. 94 (4) (2004) 462–470.
[39] C. Zeltz, J. Orgel, D. Gullberg, Molecular composition and function of integrin-based collagen glues—introducing COLINBRIs, Biochim. Biophys. Acta Gen. Subj. 1840 (8) (2014) 2533–2548.
[40] H. Zhang, L. Tian, M. Shen, C. Tu, H. Wu, M. Gu, D.T. Paik, J.C. Wu, Generation of quiescent cardiac fibroblasts from human induced pluripotent stem cells for in vitro modeling of cardiac fibrosis, Circ. Res. 125 (5) (2019) 552–566.
[41] S. Shishido, H. Bönig, Y.M. Kim, Role of integrin alpha4 in drug resistance of leukemia, Front. Oncol. 4 (99) (2014) 1–10.
[42] E.S. Welf, J.M. Haugh, Signaling pathways that control cell migration: models and analysis, Wiley Interdiscip. Rev. Syst. Biol. Med. 3 (2) (2011) 231–240.
[43] X. Zhao, J.L. Guan, Focal adhesion kinase and its signaling pathways in cell migration and angiogenesis, Adv. Drug Deliv. Rev. 63 (8) (2011) 610–615.
[44] A. Dovas, J.R. Couchman, RhoGDI: multiple functions in the regulation of Rho family GTPase activities, Biochem. J. 390 (Pt 1) (2005) 1–9.
[45] V. Talman, H. Ruskoaho, Cardiac fibrosis in myocardial infarction-from repair and remodeling to regeneration, Cell Tissue Res. 365 (3) (2016) 563–581.
[46] G.M. Fomovsky, A.D. Rouillard, J.W. Holmes, Regional mechanics determine collagen fiber structure in healing myocardial infarcts, J. Mol. Cell. Cardiol. 52 (5) (2012) 1083–1090.
[47] W. Li, Biomechanics of infarcted left ventricle: a review of modelling, Biomed. Eng. Lett. 10 (3) (2020) 387–417.
[48] J.W. Holmes, J.A. Nuñez, J.W. Covell, Functional implications of myocardial scar structure, Am. J. Phys. 272 (5 Pt 2) (1997) H2123–H2130.
[49] G.M. Fomovsky, J.R. Macadangdang, G. Ailawadi, J.W. Holmes, Model-based design of mechanical therapies for myocardial infarction, J. Cardiovasc. Transl. Res. 4 (1) (2011) 82–91.
[50] K.D. Costa, J.W. Holmes, A.D. Mcculloch, Modelling cardiac mechanical properties in three dimensions, <sb:contribution><sb:title></sb:title></sb:contribution><sb:host><sb:issue><sb:series><sb:title>Philos. Trans. R. Soc. London, Ser. A Math. Phys. Eng. Sci.</sb:title></sb:series></sb:issue></sb:host> 359 (1783) (2001) 1233–1250.
[51] W.J. Richardson, S.A. Clarke, T.A. Quinn, J.W. Holmes, Physiological implications of myocardial scar structure, Compr.Physiol. 5 (4) (2015) 1877–1909.
[52] C. Wan, Z. Hao, S. Wen, H. Leng, A quantitative study of the relationship between the distribution of different types of collagen and the mechanical behavior of rabbit medial collateral ligaments, PLoS One 9 (7) (2014), e103363.
[53] C. Cochain, K.M. Channon, J.S. Silvestre, Angiogenesis in the infarcted myocardium, Antioxid. Redox Signal. 18 (9) (2013) 1100–1113.
[54] S.D. Prabhu, N.G. Frangogiannis, The biological basis for cardiac repair after myocardial infarction: from inflammation to fibrosis, Circ. Res. 119 (1) (2016) 91–112.
[55] Y. Hadas, M.G. Katz, C.R. Bridges, L. Zangi, Modified mRNA as a therapeutic tool to induce cardiac regeneration in ischemic heart disease, Wiley Interdiscip. Rev. Syst. Biol. Med. 9 (1) (2017).
[56] A. Neve, F.P. Cantatore, N. Maruotti, A. Corrado, D. Ribatti, Extracellular matrix modulates angiogenesis in physiological and pathological conditions, Biomed. Res. Int. 2014 (2014), 756078.
[57] S. Ricard-Blum, R. Salza, Matricryptins and matrikines: biologically active fragments of the extracellular matrix, Exp. Dermatol. 23 (7) (2014) 457–463.
[58] C.D. Lawson, A.J. Ridley, Rho GTPase signaling complexes in cell migration and invasion, J. Cell Biol. 217 (2) (2018) 447–457.